Plasma sheet pressure variations in the near Earth magnetotail during substorm growth phase: THEMIS observations

W. J. Sun [1, 2, 3], S. Y. Fu [3], Y. Wei [1, 2, 4], Z. H. Yao [5], Z. J. Rong [1, 2], X. Z. Zhou [3], J. A. Slavin [6], W. X. Wan [1, 2, 4], Q. G. Zong [3], Z. Y. Pu [3], Q. Q. Shi [7], X. C. Shen [7]

Corresponding author: W. J. Sun (weijiesun@pku.edu.cn)

[1] Key Laboratory of Earth and Planetary Physics, Institute of Geology and Geophysics, Chinese Academy of Sciences, Beijing 100029, China.

[2] Institutions of Earth Science, Chinese Academy of Sciences, Beijing 100029, China.

[3] School of Earth and Space Sciences, Peking University, Beijing 100871, China.

[4] College of Earth Sciences, University of Chinese Academy of Sciences, Beijing, China.

[5] Laboratoire de Physique Atmosphérique et Planétaire, STAR Institute, Université de Liège, Liège, Belgium.

[6] Department of Climate and Space Sciences and Engineering, University of Michigan, Ann Arbor, MI, USA

[7] Shandong Provincial Key Laboratory of Optical Astronomy and Solar-Terrestrial Environment, School of Space Science and Physics, Shandong University, Weihai, China

Running title:

Plasma Sheet Pressure during SGP

Key Points:

About 40% of the selected events in the near-tail region display a phenomenon of equatorial plasma pressure decrease

An enhanced equatorial convection with speed of ~ 20 km/s is observed in our cases during the substorm growth phase

Statistical studies for the distributions of P_{eq} properties and electron pressure variations are performed

Abstract. We investigate the plasma sheet pressure variations in the near Earth magnetotail (Radius distance, R, from 7.5 R_E to 12 R_E and Magnetic Local Time, MLT, from 18:00 to 06:00) during substorm growth phase with Time History of Events and Macroscale Interactions during Substorms (THEMIS) observations. It is found that, during the substorm growth phase, about 39.4% (76/193) of the selected events display a phenomenon of equatorial plasma pressure (P_{eq}) decrease. The occurrence rates of P_{eq} decrease cases are higher in the dawn (04:00 to 06:00) and dusk (18:00 to 20:00) flanks (> 50%) than in the midnight region (20:00 to 04:00, < 40%). The mean values of the maximum percentages of P_{eq} decrease during the substorm growth phases are larger in the dawn and dusk flanks (~ - 20%) than in the midnight region (~ > - 16%). The mean value of P_{eq} increase percentages at the end of substorm growth phase is the highest (~ 40%) in the pre-midnight MLT bin (22:00 to 00:00) and is almost unchanged in the dawn and dusk flanks. Further investigations show that 13.0% of the events have more than 10% of P_{eq} decrease at the end of substorm growth phase comparing to the value before the growth phase, and ~ 28.0% of the events have small changes (< 10%), and ~ 59.0% events have a 10% increase. This study also reveals the importance of electron pressure (P_e) in the variation of P_{eq} in the substorm growth phase. The P_e variations often account for more than 50% of the P_{eq} changes, and the ratios of P_e to ion pressure often display large variations (~ 50%). Among the investigated events, during the growth phase, an enhanced equatorial plasma convection flow is observed, which diverges in the midnight tail region and propagates azimuthally towards the dayside magnetosphere with velocity of ~ 20 km/s. It is proposed that the P_{eq} decreases in the near Earth plasma sheet during the substorm growth phase may be due to the transport of closed magnetic flux towards the dayside magnetosphere driven by dayside magnetopause reconnection. Both solar wind and ionospheric conductivity effects may influence the distributions of occurrence rates for P_{eq} decrease events and the P_{eq} increase percentages in the investigated region.

1. Introduction

It is widely accepted that substorm growth phase starts with a southward turning of the interplanetary magnetic field (IMF) near the dayside magnetopause, ends with the onset of magnetic field dipolarization in the near-tail. Its typical duration is ~ 30 minutes to ~ 2 hours [e.g., *McPherron et al.*, 1973; *Russell and McPherron*, 1973; *Baker et al.*, 1996; *Li et al.*, 2013]. Southward IMF leads to the initiation of dayside magnetopause reconnection and transport of amount of magnetic flux from dayside magnetosphere to the magnetotail [*Dungey*, 1961]. The subsequent flaring of magnetotail as the lobes expand to accommodate the added flux increases the solar wind ram pressure on the magnetopause, which must be balanced by the increase of lobe magnetic pressure [e.g., *McPherron et al.*, 1973; *Russell and McPherron*, 1973]. And, in turn, the plasma sheet pressure is expected to increase to balance the enhanced lobe pressure [*Nagai et al.*, 1997; *Wang et al.*, 2004; *Kistler et al.*, 2006; *Forsyth et al.*, 2014]. Substorm growth phase is thus accompanied by many distinct features, such as the thinning of plasma sheet, increasing of the cross-tail current density, and enhanced convection in the equatorial magnetosphere. These features have been widely reported and discussed in both observations [*McPherron*, 1970, 1973; *Russell and McPherron*, 1973; *Petrukovich et al.*, 1999; *Asano et al.*, 2003] and empirical models [*Wang et al.*, 2013; *Yue et al.*, 2015]. However, there are also studies showing that the pressure increases were not evident during the growth phase of many substorm events [e.g., *Kistler et al.*, 1993; *Snekvik et al.*, 2012]. Thus, how is the plasma sheet pressure varied during the substorm growth phase is still not well understood and requires further investigations.

The average ion temperature (T_i) in the plasma sheet can be several times (~ 5 – 10) higher than the electron temperature (T_e) [e.g., *Slavin et al.*, 1985; *Baumjohann et al.*, 1989], and the ratio of T_i / T_e varies with solar wind and geomagnetic conditions [*Wang et al.*, 2012; *Grigorenko et al.*, 2016]. In many of the previous studies, electron pressure was often neglected [e.g. *Kistler et al.* 2006; *Forsyth et al.*, 2014], or assumed to be a small proportion to the ion pressure (14%) [e.g., *Petrukovich et al.*, 1999; *Snekvik et al.*, 2012], in the calculation of total plasma sheet pressure. Although there were studies considered the contribution of measured electron pressure to the total plasma sheet pressure [e.g., *Artemyev et al.*, 2016], it remains unclear how the T_i / T_e changes during the substorm growth phase. Thus, reliable *in situ* electron measurements are needed when precisely calculating the total plasma sheet pressure.

Recently, midnight magnetic flux depletion (MFD) in the near-Earth magnetotail during substorm growth phase has been studied in three-dimensional mesoscale magnetohydrodynamics (MHD) simulations [*Hsieh and Otto*, 2014, 2015; *Otto et al.*, 2015]. In the simulation, MFD was generated by the equatorial convection across the closed field lines, which was suggested to be driven by the dayside magnetopause reconnection [e.g., *Coroniti and Kennel*, 1973; *Kan*, 1990]. The equatorial convection in the simulation converged in the dayside magnetopause region and diverged in the midnight tail region. This convection was suggested to be along the contour of constant flux tube entropy, which corresponded to the region of *R* (Radius distance) from 8 R_E to 15 R_E [*Otto et al.*, 2015]. *Hsieh and Otto* [2014, 2015] further pointed out that MFD process could play an important role in the formation of thin current sheet in the near-Earth magnetotail region during substorm growth phase. The simulation works by *Hsieh and Otto* [2014, 2015] implied that MFD might be more intense than magnetic flux loading process in the near-Earth plasma sheet, which should have an impact on the evolution of plasma sheet pressure. However, these results were in theoretical or simulation context, and need to be tested and verified by *in situ* observations.

This paper aims to get better understanding of the plasma pressure variations in the near-tail plasma sheet with Time History of Events and Macroscale Interactions during Substorms (THEMIS) observations [*Angelopoulos*, 2008]. THEMIS consists of five identical probes carrying a series of similar instruments with highly elliptical orbits around the Earth. The probes provide plasma measurements for both ions and electrons. The apogees of THA, THD and THE were at ~ 12 R_E during most of their tail seasons from 2008 to 2015, except that THA apogee was at ~ 10 R_E during 2008 tail season. Spacecraft with equatorial orbits would have more chances to stay in the central plasma sheet and benefit this investigation. In this study, we present detailed observations of pressure variations during substorm growth phase in the near-Earth tail plasma sheet. We find that plasma pressure in the equatorial plane does not always increase during the time of growth phase but decrease sometimes. Further sunward convection is seen to be enhanced, and electron pressure could make a significant contribution to the equatorial plasma pressure, especially at the late growth phase. The potential mechanisms for the variation of the plasma pressure in the growth phase are also discussed.

2. Observations for equatorial plasma pressure variations

This study employs data from the identical instruments onboard the THEMIS probes. Specifically, magnetic field data from the Fluxgate Magnetometer (FGM) [*Auster et al.*, 2008], the combined ion data from Electrostatic Analyzer (ESA) [*McFadden et al.*, 2008] and the Solid State Telescope (SST), and the electron data from ESA. The magnetic field and particle data used are all spin-resolution (3 s). NASA/GSFC's OMNI data set through OMNIWeb, which is shifted to the Earth's bow shock nose [*King and Papitashvili*, 2005], is the source of solar wind conditions for the substorm growth phases examined in this study. We employ the SuperMAG provided SML auroral index, which is similar to AL [*Gjerloev*, 2012]. All quantities in this work are in Geocentric Solar Magnetospheric (GSM) coordinate system unless further notice.

2.1. Case study

We first introduce a substorm case on 5 April 2009. Figure 1 displays the overview of solar wind conditions and geomagnetic field perturbation from 0830 UT to 0930 UT. The solar wind data contain a clear IMF southward turning at ~ 0848 UT (marked by the first vertical dashed line) with the preceding IMF northward more than one hour (Figure 1c). The solar wind energy flux (ε) transported into the magnetosphere [*Perreault and Akasofu*, 1978] shows an enhancement in the period of southward IMF (Figure 1e). SuperMAG SML index [*Gjerloev*, 2012] was generally smaller than -50 nT during the same period, but decreased sharply from ~ -30 nT to ~ -230 nT at ~ 0917 UT (Figure 1f) indicating the initiation of substorm expansion phase. The onset of the expansion phase was identified to be at ~ 0917 UT based on the criteria from *Newell and Gjerloev* [2011] (the second vertical dashed line). These features show that the time interval from ~ 0848 UT to ~ 0917 UT was the growth phase of this substorm event. IMF was southward during the entire growth phase and turned northward ~ 10 minutes after the beginning of substorm expansion phase. During the growth phase, the variation of solar wind dynamic pressure was smooth and small (~ 0.3 nPa, Figure 1d), which should not be able to drive large perturbation in the magnetosphere.

Plasma and magnetic field measurements from THD in the near-tail region (~ - 11 R_E) for this event are shown in Figure 2. The first vertical dashed line corresponds to the first vertical line (southward turning of IMF) in Figure 1, marking the beginning of the growth phase. The second vertical dashed line marks the time of the high speed plasma flow arrival, followed by substorm dipolarization detected by THD. During the entire growth phase, THD was located in the central plasma sheet with $|B_x| < 10$ nT (Figure 2g), $T_i > 2$ keV (Figure 2b), $n_i > 0.3$ cm^{-3} (Figure 2d), and plasma $\beta > 5$ (ratio between thermal pressure and magnetic pressure, not shown). The differential energy fluxes for ions (Figure 2a) and electrons (Figure 2e) were mostly distributed in the region higher than ~ 1 keV, which further confirms that THD was located in the central plasma sheet. It was about 6 minutes after the IMF southward turning (~ 0854 UT) when THD observed a smooth decrease in B_z. The decrease in B_z (from ~ 6 nT to

~ 3 nT) is a natural consequence of plasma sheet thinning process, which was accompanied by the increase of $|B_x|$ (from ~ 0 nT to ~ 8 nT, Figure 2g). Meanwhile, THD observed an increase in n_i (from ~ 0.30 cm^{-3} to ~ 0.55 cm^{-3}, Figure 2d), a decrease in T_i (from ~ 5.5 keV to ~ 3 keV, Figure 2b), and a decrease in T_e (from ~ 1.9 keV to ~ 0.6 keV, Figure 2f). It needs to be noted that the off-diagonal components for ion and electron temperature tensors are much smaller than the diagonal components (*xx*, *yy*, and *zz* components shown in Figures 2b and 2f). In this case, the diagonal components for ions (T_{ixx} (black), T_{iyy} (green), T_{izz} (red), Figure 2b) and electrons (T_{exx} (black), T_{eyy} (green), T_{ezz} (red), Figure 2f) overlap indicating that T_i and T_e may be treated as scalar quantities.

Figure 3 shows the pressure variations measured by THD in the event. The four panels show the magnetic pressure of B_x and B_y components (P_{bxy}, Figure 3a), the electron *zz* component pressure (P_{ezz}, Figure 3b), the ion *zz* component pressure (P_{izz}, Figure 3c), and the plasma pressure in the equatorial plane (i.e., equatorial plasma pressure, P_{eq}, Figure 3d). The first and last vertical dashed lines correspond to the two lines in Figure 2. The middle vertical dashed line indicates the time of minimum P_{eq}. Because THD was not always located near the magnetic equator during the substorm growth phase, P_{eq} was obtained from the vertical pressure balance condition [e.g., *Xing et al.*, 2009, 2011; *Yao et al.*, 2012]. The derivation starts from

$$\nabla \cdot \overleftrightarrow{P} = \vec{J} \times \vec{B} \quad (1)$$

, where $\overleftrightarrow{P}$ is the thermal pressure tensor (including both ion, $\overleftrightarrow{P}_i$, and electron, $\overleftrightarrow{P}_e$), $\vec{J}$ the current density, and $\vec{B}$ the magnetic field. Considering Ampere's Law,

$$\nabla \times \vec{B} = \mu_0 \vec{J} \quad (2)$$

, and assuming that the weak dawn-dusk asymmetry of the magnetic field, i.e., $\partial/\partial y \sim 0$, we can integrate the force balance equation vertically from the equatorial plane, and gives

$$P_{eq} = P_{izz} + P_{ezz} + \frac{(B_x^2 + B_y^2)}{2\mu_0} - \frac{1}{\mu_0}\int_0^z \frac{\partial B_z}{\partial x} B_x dz \qquad (3)$$

, where P_{eq} is the equatorial plasma pressure. P_{izz} and P_{ezz} are the *zz* components of the locally measured ion and electron pressure tensors. B_x, B_y and B_z are the locally measured magnetic field *x*, *y*, and *z* components. The fourth term on the right hand side is the curvature force, which has been calculated in models [*Xing et al.*, 2009] and observations [*Xing et al.*, 2011]. The curvature force has proved to be much smaller than thermal pressure when the observing satellite was located in the central plasma sheet. Therefore, this term can be ignored by comparison to the other three terms [e.g., *Xing et al.*, 2009, 2011]. During the entire growth phase for this substorm event, β at THD was always larger than 5. Thus, we have neglected the curvature force term in the calculation of P_{eq}. THD observation shows that P_{bxy} was small during the growth phase, and increased from ~ 0 to ~ 0.025 nPa. P_{ezz} also showed some variations with a decrease from ~ 0.14 nPa to ~ 0.08 nPa. Both P_{izz} and P_{eq} decreased at the beginning of the growth phase but increased at a later time. The decrease of P_{eq} was from ~ 0.41 nPa to ~ 0.325 nPa (~ 0.085 nPa, ~ 20.7 %), while the increase was from ~ 0.325 nPa to ~ 0.35 nPa (~ 0.085 nPa, ~ 7.7 %). The standard deviation of P_{eq} variations prior to the substorm growth phase (from 0818 UT to 0848 UT) was very small (~ 2.3%) compared to the P_{eq} variations during the period of growth phase. Thus this event clearly shows that the equatorial plasma pressure in the near Earth plasma sheet could decrease during the substorm growth phase.

2.2. Event Selections

The case displayed in the previous section revealed a P_{eq} decrease process preceding P_{eq} increases in substorm growth phase. However, in addition to this case result, a statistical analysis to reveal the common features of P_{eq} variations in the near-Earth tail region throughout the growth phase is clearly required. THA, THD and THE data during the tail seasons from 2007 and 2015 (including durations from December 1

2007 to April 30 2008, December 1 2008 to April 30 2009, March 1 2010 to May 31 2010, March 1 2011 to June 30 2011, April 1 2012 to October 31 2012, June 1 2013 to September 30 2013, June 29 2014 to October 31 2014, and August 31 2015 to December 31 2015) were surveyed to search for the events of interest according to the following procedures.

1). The first step is to select the IMF southward turning events based on one minute OMNI dataset. The preceding IMF before southward turning should be mostly (> 85%) northward with an interval longer than 60 minutes, and the following IMF after southward turning should be mostly (> 85%) southward with an interval longer than 30 minutes. The average value of B_z minus the standard deviation of B_z during the 60 minutes period should be greater than zero for the preceding IMF, and the average value of B_z plus the standard deviation of B_z during the 30 minutes period should be smaller than zero for following IMF. In addition, the variation of solar wind dynamic pressure (D_p) should be small to exclude the influence from D_p changes on magnetotail dynamics. Here we use the criterion that the standard deviation of D_p during the 90 minutes (60 minutes preceding and 30 minutes following) is smaller than 30% of the average D_p.

2) The second step is to further select the isolated substorm events from the IMF southward turning events. The SuperMAG SML index [*Gjerloev*, 2012] and substorm onset lists from *Newell and Gjerloev* [2011] and *Forsyth et al.* [2015] (a specified expansion phase threshold of 50%) are employed in the selection. The preceding period should be with average value of SML greater than – 100 nT in one hour, and there should be no substorm onsets listed by *Newell and Gjerloev* [2011] and *Forsyth et al.* [2015]. The minimum SML index after IMF southward turning should be smaller than – 150 nT in the following three hours. Substorm expansion phase is identified to begin with a rapid decrease of SML (dSML/dt < – 4 nT/min).

We refer to *Li et al.* [2013] for the selection of IMF southward turning events, and *Juusola et al.* [2011] and *Li et al.* [2013] for the selection of substorms and the beginning time of substorm expansion phase. Substorm growth phase is defined to be the period between IMF southward turning point and the first point satisfying dSML/dt < - 4 nT/min. If a probe detected a dipolarization in the plasma sheet after the IMF southward turning, but before the time satisfying dSML/dt < - 4 nT/min, the beginning of expansion phase is then defined to be the moment when spacecraft observed the dipolarization. Figures 2 and 3 show an event that THD detected dipolarization and flow bursts, which was defined as the beginning of substorm expansion phase. Nevertheless, in observations, spacecraft does not always detect the dipolarization and flow bursts at the substorm onset, especially when spacecraft is located in the near flank regions (Magnetic Local Times, MLTs from ~ 3:00 to 6:00 and ~ 18:00 to 21:00). Figures 4a to 4f display one of this kind. The first vertical line indicates the beginning of substorm growth phase, i.e., southward turning of IMF, and the second vertical line indicates the first point satisfying dSML/dt < - 4 nT/min. This period is defined to be the substorm growth phase based on our criteria. The stretching (B_x increase) and flaring (B_y increase) of the magnetic field lines can be clearly observed (Figure 4f), while B_z decreases at first and then increases slightly. After the beginning of expansion phase, there is a clearly decrease in P_{eq}, which is consistent with the signatures of substorm expansion phase. It can be seen that our criteria for the selection of substorm growth phase events also works well for the cases measured near the flanks. (Data Set DS01 in the supporting information shows the list of the growth phases, containing the start times and end times of the events)

3). The last step is to exclude the influences from other effects. Probe should be located in the region with $R > 7.5\ R_E$ ($R = \sqrt{X_{GSM}^2 + Y_{GSM}^2}$), as plasmapause position could reach to ~ 7.5 R_E during quite period [*Moldwin et al.*, 2002; *Liu and Liu*, 2014]. Besides, Probe is required to be located in the inner plasma sheet with β > 0.5 during most of the time (> 85%) in growth phase. This aims to obtain accurate estimation of

P_{eq} as introduced in Section 2.1. Furthermore, the events associated with multi-crossings of current sheet are excluded, such as, those accompanied with current sheet flapping waves. The current sheet flapping waves are believed to be generated by magnetic gradient instability [e.g., *Sun et al.*, 2014; *Korovinskiy et al.*, 2015], which should be in association with pressure gradients. In addition, to avoid the influence from localized dipolarizations, we have also eliminated those events that observed dipolarization signatures (B_z increase) in one hour prior to the IMF southward turning. Finally, we exclude as well the cases that the plasma sheet with large disturbance prior to the substorm growth phase. For this purpose, we calculate the standard deviation for plasma sheet P_{eq} in the period of half an hour prior to the growth phase (δP_{eq}), which should be much smaller (< 5%) than the mean value of P_{eq} in the same period.

Following the whole procedure, a total of 193 cases are selected. There are many observations similar to the case shown in Section 2.1 with P_{eq} decrease, and there are also many cases associated with clear P_{eq} increase in the entire substorm growth phase analogous to the previous observations [e.g., *Nagai et al.*, 1997; *Wang et al.*, 2004; *Kistler et al.*, 2006]. Figures 4g to 4l show an event with P_{eq} increase during the entire growth phase. The two vertical dashed lines represent the beginning and end of the substorm growth phase. The plasma sheet thinning and magnetic field line stretching and flaring, including B_z decrease, B_x and B_y increase (Figure 4l), are clearly seen. For this case, the increase of P_{eq} was from ~ 0.27 nPa to ~ 0.37 nPa (~ 37%, Figure 4k). In the following section, P_{eq} variations during the substorm growth phase will be discussed in detail.

2.3. Statistical Results

Among the 193 cases selected, in 76 of them (~ 39.4%) certain amount of P_{eq} decrease (hereafter call P_{eq} decrease case) was observed. This study defines (P_{eqmin} -

P_{eq0}) / $\delta P_{eq} \geq 3$, where P_{eqmin} is the minimum of P_{eq} during the growth phase, P_{eq0} the P_{eq} before the start of growth phase, and δP_{eq} is the standard deviation of P_{eq} in the period of half an hour prior to the substorm growth phase. The selection of P_{eqmin} is based on one minute moving mean P_{eq} data, where the decrease in P_{eq} should be relatively steady. We determined from the differences between adjacent data points, which should be constantly negative in a period longer than five minutes before the data point of P_{eqmin}. This near ~ 40% occurrence rate suggests that the P_{eq} decrease phenomenon in the near-tail plasma sheet during the substorm growth phase is common. The distribution of 193 probe observations in X_{GSM}-Y_{GSM} plane is shown in Figure 5. Blue circles represent the locations of P_{eq} decrease cases, and red circles represent others. The black arrows in Figure 5a represent the averaged plasma flows in X_{GSM}-Y_{GSM} plane ($\vec{V}_{xy} = V_x\vec{e}_x + V_y\vec{e}_y$) , and the black arrows in Figure 5b indicate the differences between the flows in Figure 5a and the averaged plasma flows in half an hour prior to the growth phase. The statistical features on P_{eq} variations for all the events will be further investigated in Figure 6. Here we discuss the plasma flow properties.

In the midnight magnetic flux depletion (MFD) model, the closed magnetic flux tubes, which could be transported into dayside and balance the reconnection eroded magnetic flux, should hold the same entropy as the dayside magnetopause [*Otto et al.*, 2015; *Hsieh and Otto*, 2015]. The MFD region is estimated to be located in the near-Earth tail from around R = - 8 R_E to - 15 R_E [*Otto et al.*, 2015]. In this study, we focus on the tail region between R = - 7.5 R_E and R = - 12 R_E. The equatorial plasma flows in our cases are mostly along the tangential directions of different R circles, which are very likely along the contours of constant flux tube entropy as shown in [*Otto et al.*, 2015], and diverge in the near midnight tail region (Figure 5a). This convection divergence in the midnight tail is also similar to the velocity distributions shown in the MHD simulations [*Otto et al.*, 2015; *Hsieh and Otto*, 2015]. This plasma convection flow provides strong evidence for the existence of equatorial convection which is consistent with the picture of MFD. The plasma convection flow velocities are observed to be around 20 km/s. Figure 5b displays the plasma flow differences ($\Delta\vec{V}_{xy}$) between the average plasma flows during substorm growth phase and the flows in half an hour prior to the substorm growth phase, which clearly shows the enhancements of around 10 km/s of plasma flows towards the dayside.

To investigate the spatial distribution of the P_{eq} variations, Figure 6 shows the statistical features on the 193 cases. Figure 6a shows the occurrence rates for P_{eq} decrease cases in different Magnetic Local Time (MLT) bin. In this figure, each MLT bin includes two magnetic local hours to make sure each bin contains enough cases (> 10). The occurrence rates of P_{eq} decrease cases are ~ 50% for the dawn MLT bin (04:00 to 06:00), and ~ 80% for the dusk MLT bin (18:00 to 20:00), respectively, but are < 40% in the other four midnight MLT bins (20:00 to 22:00, 22:00 to 00:00, 00:00 to 02:00, 02:00 to 04:00). This figure indicates that the P_{eq} decrease cases are more often observed in the dawn and dusk flanks rather than midnight tail region. Figure 6b has investigated the distributions of percentages of P_{eq} decrease along the MLT bins. We have calculated the ratios of P_{eq} decrease (($P_{\mathrm{eqmin}} - P_{\mathrm{eq0}}$) / P_{eq0}) for each case. Determinations of P_{eqmin} and P_{eq0} were introduced above. Cases that do not observe P_{eq} decrease are excluded. The P_{eq} decrease percentage distributions (Figure 6b) indicate that the mean percentages in dawn (04:00 to 06:00 and 02:00 to 04:00, ~ - 20%) and dusk (18:00 to 20:00, ~ - 18%) MLT bins are smaller than the midnight MLT bins (> - 16%), indicating that the P_{eq} decrease is more prominent in the dawn and dusk flanks than the midnight regions. We note the P_{eq} decrease percentage distributions that include the cases do not observe P_{eq} decrease (not shown) give the similar feature as Figure 6b, but with the mean percentages in each MLT bins larger (> - 15%).

In Figure 6c, we have further investigated P_{eq} increase ratios (($P_{\mathrm{eqend}} - P_{\mathrm{eq0}}$) / P_{eq0}) at the end of substorm growth phase, where P_{eqend} is the P_{eq} at the end of substorm growth phase. Figure 6c shows that the mean ratios of P_{eq} increase is the highest in the pre-midnight MLT bin (22:00 to 00:00, ~ 40%). And the mean of P_{eq} increase ratios are decreasing towards the dawn and dusk flanks, with the average P_{eq} almost unchanged (~ 0%) in the dawn and dusk flank MLT bins. Green circles in Figure 6c are the scatter of P_{eq} increase ratios for the 193 cases. This scatter shows that in many cases P_{eq} at the end of substorm growth phase could smaller than P_{eq0}. To further evaluate this phenomenon, we have divided the cases into three groups. The first group contains events satisfying $(P_{eqend} - P_{eq0}) / P_{eq0} < -10\%$, the second group satisfying $|(P_{eqend} - P_{eq0}) / P_{eq0}| < 10\%$, and the third group $(P_{eqend} - P_{eq0}) / P_{eq0} > 10\%$. There are 25 events (25/193, ~ 13.0%) in the first group, which means that P_{eq} decreases more than 10% in ~ 13.0% of our events at the end of substorm growth phase comparing to the P_{eq} at the beginning of substorm growth phase. There are 54 events in the second group, indicating that in ~ 28.0% (54/193) of our events P_{eqend} is similar to P_{eq0}. The third group contains 114 events, indicating that ~ 59.0% of the events display large P_{eq} increase at the end of substorm growth phase.

We have further investigated the relationship between the three groups of events and the P_{eq} decrease events. Twenty-four of the 25 events (~ 96%) in the first group are the P_{eq} decrease events, 26 of the 54 events (~ 48.1%) in the second group are the P_{eq} decrease events, and 26 of the 114 events (~ 22.8%) in the third group are the P_{eq} decrease events. The events in the first group corresponding to more than 10% P_{eq} decrease at the end of substorm growth phase are highly correlated with the P_{eq} decrease events (~ 96%). And this percentage drops to ~ 22.8% in the third group. This clearly indicates that P_{eq} decrease events more often correspond to P_{eq} decrease at the end of substorm growth phase, but there are still some events corresponding to more than 10% of P_{eq} increase at the end of substorm growth phase.

3. Electron pressure contribution

In many previous studies, the contribution of P_e to the total pressure was neglected [e.g., *Kistler et al.*, 2006; *Forsyth et al.*, 2014] or assumed to be only a small portion (14%) of the P_i [e.g., *Petrukovich et al.*, 1999; *Snekvik et al.*, 2012] during substorm growth phase in the tail plasma sheet. However, the cases in Figures 3 and 4 showed that P_{ezz} or P_{bxy} displayed large variations in the growth phase. In Figure 3, P_{ezz} exhibited a decrease of ~ 0.06 nPa in the growth phase (Figure 3b), and P_{bxy} showed an increase of ~ 0.025 nPa (Figure 3a) at the same time, which were comparable with the increase of P_i (~ 0.04 nPa, Figure 3c). For the case in Figures 4g to 4l, P_{eq} increment (~ 0.1 nPa, Figure 4k) was almost evenly contributed by P_{izz} (Figure 4j) and P_{bxy} (Figure 4h), but with P_{ezz} (Figure 4i) being almost constant. In these two cases, because the variations of P_{bxy} were comparable to P_{izz}, the real contributions from P_{ezz} and P_{izz} to P_{eq} are not clear. Therefore, it is necessary to exclude the influence from P_{bxy} for the investigation of P_{ezz} and P_{izz} contributions to P_{eq}. We have set up the following criteria to further select events from the 193 cases:

1). $P_{bxy} \leq P_{ezz} / 5$ during the entire substorm growth phase.

2). P_{ezz} changes ($|\Delta P_{ezz}|$) should be at least five times larger than P_{bxy} changes ($|\Delta P_{bxy}|$) during the same time, i.e., $|\Delta P_{bxy}| \leq |\Delta P_{ezz}| / 5$.

It has been shown that particle distribution functions can vary even in the central plasma sheet ($\beta > 1$), especially for electrons [*Walsh et al.*, 2011]. The two criteria described above ensure the main contributors to the P_{eq} are electron and ion thermal pressure, which helps to mitigate the influence of particle distribution variations in the plasma sheet.

Among the 193 cases there are 19 cases satisfying the above constraints. Figure 7 shows an example on 20 January 2008. In this case, substorm growth phase started at ~ 0242 UT and ended at ~ 0305 UT. P_{ezz} (> 0.1 nPa, Figure 7c) was generally 10 times larger than P_{bxy} (< 0.01 nPa, Figure 7b) during the entire growth phase period. P_{eq} showed a decrease prior to the increase, similar to the case in Section 2.1. The decrease of P_{eq} was from ~ 0.35 nPa to ~ 0.29 nPa (~ 17.1%, ΔP_{eq} ~ 0.06 nPa), and increase was from ~ 0.29 nPa to ~ 0.33 nPa (~ 13.8%, ΔP_{eq} ~ 0.04 nPa). During the P_{eq} decrease stage (between the first and second vertical dashed lines), P_{ezz} showed small variation (~ 0.01 nPa) with the ratios of P_{ezz} to P_{izz} ranging from ~ 50% to ~ 55%. In the P_{eq} increase stage (between the second and third vertical dashed lines), P_{ezz} showed an increase from ~ 0.105 nPa to ~ 0.155 nPa (ΔP_{ezz} ~ 0.05 nPa) which was comparable (~ 100%) with ΔP_{eq} changes at the same time. ΔP_{bxy} (~ 0.003 nPa) was about an order smaller than ΔP_{ezz}. Ratios of P_{ezz} to P_{izz} increased from ~ 50% to ~ 80% (30%, Figure 7f) at the meantime. The above observations reveal two important features. One is that P_{ezz} variations can be comparable with that of P_{eq}. The other is that the ratios of P_{ezz} to P_{izz} can exhibit large variations. These features become prominent in the P_{eq} increase stage, i.e., the late growth phase, for this case.

Pressure variations for the selected 19 cases during substorm growth phase cases are summarized in Table 1. The ΔP_{bxy} (in nPa, fourth column), ΔP_{ezz} (in nPa, fifth column), ΔP_{eq} (in nPa, sixth column), ΔP_{izz} (in nPa, seventh column) and $\Delta(P_{ezz}/P_{izz})$ (eighth column) are the differences between the maxima and minima of each quantity during the entire substorm growth phase. The positive values mean that the quantities increase and negative values mean the quantities decrease. These multi-case results generally confirm the two features obtained from the case in Figure 7. Firstly, P_{ezz} variations could frequently account for large portion of the P_{eq} changes during the growth phase. From this table, it can be seen that ΔP_{ezz} are generally comparable with or larger than $\Delta P_{eq,}$ with the ratios of ΔP_{ezz} to ΔP_{eq} in most cases being larger than 50% (except events #4, #8, #16, and #18). Secondly, the ratios of the P_{ezz} to P_{izz} display large variations. As shown in the eighth column, P_{ezz}/P_{izz} show changes larger than 50% in about half of the events (9/19). This result indicates, firstly, the ratios between P_{ezz} and P_{izz} are not constant; secondly, P_{ezz} could be comparable with P_{izz} during substorm growth phase in the plasma sheet. We note that P_{ezz} exhibits large variations mainly in the late growth phase for most of the events.

We have further investigated the 15 cases of large electron pressure contributions (with the ratios of ΔP_{ezz} to ΔP_{eq} larger than 50%) in the X_{GSM}-Y_{GSM} plane (in Figure 8), which shows 10 of them were located in the dawnside of the magnetotail ($Y_{GSM} < 0$), and 5 of them located in the duskside ($Y_{GSM} > 0$). It seems that the events with large electron pressure contributions could be more frequently observed in the dawnside than duskside. But it needs to note that this distribution only includes 15 events. Further investigation with more events are needed to confirm this conclusion. The relationship between these 15 events and three groups for P_{eqend} variations has been shown in the ninth column in Table 1. 10 of the 15 cases (~ 66.7%) are corresponding to the third group events, 3 events corresponding to the second group events (~ 20.0%), and 2 events corresponding to the first group. The occurrence rates for each group events in the 15 cases are comparable with the percentage of the statistical result for all cases. This indicates that the occurrence of large electron pressure variations does not show obvious preferences in any groups.

4. Conclusion and Discussion

Our analyses of the THEMIS observations have revealed new features of the plasma pressure variations in the near-Earth tail region during the substorm growth phase, which are summarized below.

1. It is quite common for P_{eq} to decrease in the near-tail plasma sheet (i.e. R ~ 7.5 R_E to ~ 12 R_E) in the substorm growth phase. Such a decrease was detected in about 40% of our cases (~ 39.4%, 76/193).

2. Near the magnetic equator enhanced azimuthal convection with speeds of ~ 20

km/s along the contours of constant flux tube entropy is observed during substorm growth phase. This flow diverges in the midnight region and converges at the flanks toward the dayside.

3. The occurrence rate of P_{eq} decrease cases is higher at the dawn and dusk flanks (> 50%) than midnight (< 40%) tail region. Further, the mean P_{eq} decrease percentage is larger at the dawn and dusk flanks (~ - 20%) than in the midnight region (~ > - 16%).

4. The P_{eq} increase percentage at the end of substorm growth phase is the highest in the pre-midnight MLT bin (~ 40% from 22:00 to 00:00), and the mean of P_{eqend} almost does not change when compared to P_{eq0} in the dawn and dusk flank MLT bins. More detailed examination reveals that ~ 13.0% (25/193) of the events show a P_{eqend} decrease of more than 10% of P_{eq0} ((P_{eqend} - P_{eq0}) / P_{eq0} < - 10%, the first group), ~ 28.0% (54/193) display only a small change (|(P_{eqend} - P_{eq0}) / P_{eq0}| < 10%, the second group), and for ~ 59.0% (114/193) of the events P_{eqend} increases by more than 10% of P_{eq0} ((P_{eqend} - P_{eq0}) / P_{eq0} > 10%, the third group).

5. The P_{eq} decrease cases are highly correlated with the first group events, i.e., those with a P_{eqend} decrease of more than 10% of P_{eq0}, but there are still many P_{eq} decrease cases with a P_{eqend} increase of more than 10% of P_{eq0}. And ~ 22.8% (26/114) of the events in third group exhibit P_{eq} decreases.

6. Finally, our study has revealed that P_{ezz} variations frequently (~78.9%, 15/19) account for large portion (> 50 %) of the P_{eq} changes, and the ratios of the P_{ezz} to P_{izz} display large variations (~ 50%) with P_{ezz} being comparable with P_{izz} in about half of the events (9/19). These P_{ezz} variations occurred mainly in the late substorm growth phase. The distribution of events with large P_{ezz} variations shows they are more frequently observed in the dawnside than duskside, and the occurrence of large electron pressure variations do not display obvious preferences in any groups. With

only 15 cases, these two conclusions certainly need further investigation.

The transmission of enhanced electric fields associated with dayside magnetopause reconnection across the open field lines of the magnetotail has been extensively studied [e.g., *McPherron et al.*, 1973; *Russell and McPherron*, 1973]. The enhanced electric field due to solar wind convection transports reconnected (i.e. "open") magnetic flux from the dayside into lobes and has been believed to be responsible for an increase in total pressure in the plasma sheet [e.g., *Wang et al.*, 2004; *Kistler et al.*, 2006; *Forsyth et al.*, 2014; *Yue et al.*, 2015]. However, it has also been suggested that this enhanced electric field will be reflected in the closed field line region of the near-tail through compression and rarefaction waves [*Coroniti and Kennel*, 1973; *Kan*, 1990]. The net effect is the transport of closed magnetic flux in the near-Earth tail region to dayside magnetosphere creating a magnetic flux depletion (MFD) on the nightside [*Hsieh and Otto*, 2014, 2015; *Otto et al.*, 2015]. *Kan* [1990] further proposed that the enhanced electric field across the closed field lines arriving at the near-tail plasma sheet could be earlier than across open field lines. The simulation works of *Hsieh and Otto* [2014,2015] considers the intensity of the two processes but not their time sequences.

Given our results indicating that a P_{eq} decrease in the plasma sheet is quite common, it is inferred that MFD may indeed take place at the investigated region (R ~ 7.5 R_E to ~ 12 R_E) during the growth phase and that it could dominate the pressure balance in this region. Simulations have suggested that the transport of near-Earth magnetic flux from the nightside to the dayside should take place along contours of constant entropy [*Otto et al.*, 2015]. An equatorial convection with speed of ~ 20 km/s is observed in our cases. These plasma flows are mostly azimuthal and the flow is away from local midnight toward the dawn and dusk flanks, which does indeed follow approximately the contours of constant flux tube entropy. We believe this plasma flow convection provides strong evidence for the existence of dayside convection supporting the MFD pressure variation scenario. Accordingly, the P_{eq} decrease growth phase phenomenon reported here constitutes evidence that the plasma sheet thinning in the near tail region is not be only due to the enhanced electric field across open field lines, but also across closed field lines.

Our statistical analyses have shown that the occurrence rates for events with P_{eq} decrease near the magnetic equator are higher in the dawn and dusk flanks (> 50%) than at midnight (< 40%). They have revealed that although ~ 59.0% of our events correspond to a P_{eqend} increase, there are still events with P_{eqend} almost unchanged (~ 28.0%) or even decreasing (~ 13.0%) as compared to P_{eq0}. We believe these results may provide an explanation for the previous conflicting results concerning plasma sheet pressure variations, i.e., some showing plasma sheet pressure increase during the substorm growth phase [e.g., *Nagai et al.*, 1997; *Wang et al.*, 2004; *Kistler et al.*, 2006; *Forsyth et al.*, 2014], while others found little or no change [e.g., *Kistler et al.*, 1993; *Snekvik et al.*, 2012]. We have found that the P_{eq} increase percentage at the end of growth phase is the highest in the pre-midnight MLT bin (22:00 to 00:00). This location is in agreement with the statistical substorm onset locations at MLT ~ 21:00 to ~ 01:00 [e.g., *Liou et al.*, 2001; *Frey et al.*, 2004]. Since the variations of P_{eq} are suggested to be closely related to enhanced electric fields associated with dayside magnetopause reconnection transmitting through different paths, P_{eq} variations in the tail plasma sheet should depend on the solar wind condition and ionospheric conductance distribution in the polar region [e.g., *Kan*, 1990; *Lopez et al.*, 2014]. Simulation results have shown that plasma sheet evolution in the near-tail region should depend on the competition between the depletion of closed magnetic flux and addition of open flux, but with the open flux being added more uniformly to the magnetotail [*Hsieh and Otto*, 2015]. But there are also many studies showing that magnetic flux is often added non-uniformly to the tail due to IMF B_y influence [e.g., *Liou and Newell*, 2010; *Østgaard et al.*, 2011]. Ionospheric conductivity has also been suggested to be affected by dipole tilt [e.g., *Liou and Newell*, 2010]. How all of these processes influence this P_{eq} evolution during substorm growth phase is a very complex problem that needs further investigation.

Our results have shown that the P_{eq} changes observed during substorm growth phase frequently contain large (> 50%) contributions from $P_{ezz.}$ This result and the finding of large variations in the ratios of P_{ezz} to P_{izz} challenge the results of some previous studies and common assumptions about tail plasmas. Our results further indicate that understanding the role of electron properties is essential to understanding magnetotail pressure variations during substorm growth phase. In particular, the case studies presented here indicate that the variations in P_{ezz} are frequently very important in the late growth phase. It is at this point that the plasma sheet thins to an ion inertial length or less. Under these conditions it is not surprising that electrons are often observed to be the main contributor to the enhanced current density [e.g., *Mitchell et al.*, 1990; *Asano et al.*, 2003]. For all of these reasons we think that variation in P_{ezz} during substorm growth phase requires further investigation.

Acknowledgement.

We acknowledge NASA contract NAS5-02099 and V. Angelopoulos for use of data from the THEMIS Mission (available at http://themis.ssl.berkeley.edu/.). Specifically: D. Larson and R. P. Lin for use of SST data, C. W. Carlson and J. P. McFadden for use of ESA data, K. H. Glassmeier, U. Auster and W. Baumjohann for the use of FGM data provided under the lead of the Technical University of Braunschweig and with financial support through the German Ministry for Economy and Technology and the German Center for Aviation and Space (DLR) under contract 50 OC 0302. We also acknowledge use of NASA/GSFC's Space Physics Data Facility's OMNIWeb service (OMNI data from http://omniweb.gsfc.nasa.gov/) and the SuperMAG, PI Jesper W. Gjerloev (SML data from http://supermag.jhuapl.edu/). Wei-Jie Sun is funded by National Postdoctoral Program for Innovative Talents (grant BX201600158) and China Postdoctoral Science Foundation (grant 2016M600124). This work is supported by the National Nature Science Foundation of China (grants 41704163, 41525016, 41474155, 41474139, 41661164034 and 41274167). Yong Wei is supported by Thousand Young Talents Program of China. Zhonghua Yao is a Marie-Curie COFUND postdoctoral fellow at the University of Liège, Co-funded by the European Union. Wei-Jie Sun thanks Dr. Wenlong Liu (Beihang University, China) and Dr. Yasong Ge (Key Laboratory of Earth and Planetary Physics, Institute of Geology and Geophysics, Chinese Academy of Sciences) for helpful discussions.

References

Angelopoulos, V. (2008), The THEMIS Mission, *Space Sci Rev 141*(1-4), 5-34.

Artemyev, A. V., V. Angelopoulos, A. Runov, and A. A. Petrokovich (2016), Properties of current sheet thinning at x ~ - 10 to - 12 R_E, *J Geophys Res: Space Physics*, 121, 6718–6731.

Asano, Y., T. Mukai, M. Hoshino, Y. Saito, H. Hayakawa, and T. Nagai (2003), Evolution of the thin current sheet in a substorm observed by Geotail, *J Geophys Res: Space Physics*, *108*(A5), 1189.

Auster, H. U., et al. (2008), The THEMIS Fluxgate Magnetometer, *Space Sci Rev*, *141*(1-4), 235-264.

Baker, D. N., T. I. Pulkkinen, V. Angelopoulos, W. Baumjohann, and R. L. McPherron (1996), Neutral line model of substorms: Past results and present view, *J Geophys Res: Space Physics*, *101*(A6), 12975-13010.

Baumjohann, W., G. Paschmann, and C. A. Cattell (1989), Average plasma properties in the central plasma sheet, *J Geophys Res: Space Physics*, 94(A6), 6597-6606.

Coroniti, F. V., and C. F. Kennel (1973), Can the ionosphere regulate magnetospheric convection? *J Geophys Res*, *78*(16), 2837-2851.

Dungey, J. W. (1961), Interplanetary magnetic field and the auroral zones, *Phys. Rev. Lett.*, 6, 47–48.

Forsyth, C., et al. (2014), Increases in plasma sheet temperature with solar wind driving during substorm growth phases, *Geophys Res Lett*, *41*(24), 8713-8721.

Forsyth, C., I. J. Rae, J. C. Coxon, M. P. Freeman, C. M. Jackman, J. Gjerloev, and A. N. Fazakerley (2015), A new technique for determining Substorm Onsets and Phases from Indices of the Electrojet (SOPHIE), *J. Geophys. Res. Space Physics*, 120, 10,592–10,606, doi:10.1002/2015JA021343.

Frey, H. U., S. B. Mende, V. Angelopoulos, and E. F. Donovan (2004), Substorm onset observations by IMAGE-FUV, *J. Geophys. Res. Space Physics*, 109, A10304, doi:10.1029/2004JA010607. Gjerloev, J. W. (2012), The SuperMAG data processing technique, *J. Geophys. Res.*, 117, A09213, doi:10.1029/2012JA017683.

Grigorenko, E. E., E. A. Kronberg, P. W. Daly, N. Y. Ganushkina, B. Lavraud, J. A. Sauvaud, and L. M. Zelenyi (2016), Origin of low proton-to-electron temperature ratio in the Earth's plasma sheet, *J Geophys Res: Space Physics*, 121(10), 9910-9985.

Hsieh, M. S., and A. Otto (2014), The influence of magnetic flux depletion on the magnetotail and auroral morphology during the substorm growth phase, *J Geophys Res: Space Physics*, *119*(5), 3430-3443.

Hsieh, M. S., and A. Otto (2015), Thin current sheet formation in response to the loading and the depletion of magnetic flux during the substorm growth phase, *J Geophys Res: Space Physics*, *120*(6), 4264-4278.

Juusola, L., N. Østgaard, E. Tanskanen, N. Partamies, and K. Snekvik (2011), Earthward plasma sheet flows during substorm phases, *J Geophys Res*: *Space Physics*, 116(A10), n/a-n/a.

Kan, J. R. (1990), Tail-like reconfiguration of the plasma sheet during the substorm growth phase, *Geophys Res Lett*, *17*(13), 2309-2312.

King, J. H., and N. E. Papitashvili (2005), Solar wind spatial scales in and comparisons of hourly Wind and ACE plasma and magnetic field data, *J Geophys Res: Space Physics*, *110*(A2), A2104.

Kistler, L. M., W. Baumjohann, T. Nagai, and E. Möbius (1993), Superposed epoch analysis of pressure and magnetic field configuration changes in the plasma sheet, *J Geophys Res: Space Physics*, *98*(A6), 9249-9258.

Kistler, L. M., et al. (2006), Ion composition and pressure changes in storm time and nonstorm substorms in the vicinity of the near-Earth neutral line, *J Geophys Res: Space Physics*, *111*(A11222A11).

Korovinskiy, D. B., A. V. Divin, N. V. Erkaev, V. S. Semenov, A. V. Artemyev, V. V. Ivanova, I. B. Ivanov, G. Lapenta, S. Markidis, and H. K. Biernat (2015), The double-gradient magnetic instability: Stabilizing effect of the guide field, *Physics of Plasmas (1994-present)*, 22(1), 12904.

Li, H., C. Wang, and Z. Peng (2013), Solar wind impacts on growth phase duration and substorm intensity: A statistical approach, *J Geophys Res: Space Physics*, *118*(7), 4270-4278.

Liou, K., P. T. Newell, D. G. Sibeck, C. I. Meng, M. Brittnacher, and G. Parks (2001), Observation of IMF and seasonal effects in the location of auroral substorm onset, *Journal of Geophysical Research: Space Physics*, 106(A4), 5799-5810.

Liou, K., and P. T. Newell (2010), On the azimuthal location of auroral breakup: Hemispheric asymmetry, *Geophys Res Lett*, 37(23), L23103.

Liu, X., and W. Liu (2014), A new plasmapause location model based on THEMIS observations, *Science China Earth Sciences*, 57(10), 2552-2557.

Lopez, R. E., R. Bruntz, and K. Pham (2014), Linear separation of orthogonal merging component and viscous interactions in solar wind-geospace coupling, *J Geophys Res: Space Physics*, *119*(9), 7566-7576.

McFadden, J. P., C. W. Carlson, D. Larson, M. Ludlam, R. Abiad, B. Elliott, P. Turin, M. Marckwordt, and V. Angelopoulos (2008), The THEMIS ESA Plasma Instrument and In-flight Calibration, *Space Sci Rev*, *141*(1-4), 277-302.

McPherron, R. L. (1970), Growth phase of magnetospheric substorms, *J Geophys Res*, *75*(28), 5592-5599.

McPherron, R. L., C. T. Russell, and M. P. Aubry (1973), Satellite studies of magnetospheric substorms on August 15, 1968: 4. Ogo 5 magnetic field observations, *J. Geophys. Res.*, 78(16), 3068–3078.

Mitchell, D. G., D. J. Williams, C. Y. Huang, L. A. Frank, and C. T. Russell (1990), Current carriers in the near-Earth cross-tail current sheet during substorm growth phase, *Geophys Res Lett*, 17(5), 583-586.

Moldwin, M. B., L. Downward, H. K. Rassoul, R. Amin, and R. R. Anderson (2002), A new model of the location of the plasmapause: CRRES results, *Journal of Geophysical Research: Space Physics*, 107(A11), 1-2.

Nagai, T., T. Mukai, T. Yamamoto, A. Nishida, S. Kokubun, and R. P. Lepping (1997), Plasma sheet pressure changes during the substorm growth phase, *Geophys Res Lett*, *24*(8), 963-966.

Newell, P. T., and J. W. Gjerloev (2011), Evaluation of SuperMAG auroral electrojet indices as indicators of substorms and auroral power, *J. Geophys. Res.*, 116, A12211, doi:10.1029/2011JA016779.

Østgaard, N., K. M. Laundal, L. Juusola, A. Åsnes, S. E. Håland, and J. M. Weygand (2011), Interhemispherical asymmetry of substorm onset locations and the interplanetary magnetic field, *Geophys Res Lett*, 38(8), n/a-n/a.

Otto, A., Hsieh, M.-S. and Hall, F. (2015) Current Sheets Formation in Planetary Magnetotail, in *Magnetotails in the Solar System* (eds A. Keiling, C. M. Jackman and P. A. Delamere), *John Wiley & Sons, Inc*, Hoboken, NJ. doi: 10.1002/9781118842324.ch17

Perreault, P., and S. I. Akasofu (1978), A study of geomagnetic storms, *Geophys J Int*, *54*(3), 547-573.

Petrukovich, A. A., T. Mukai, S. Kokubun, S. A. Romanov, Y. Saito, T. Yamamoto, and L. M. Zelenyi

(1999), Substorm-associated pressure variations in the magnetotail plasma sheet and lobe, *J Geophys Res: Space Physics*, *104*(A3), 4501-4513.

Russell, C. T., and R. L. McPherron (1973), The magnetotail and substorms, *Space Sci Rev*, *15*(2-3), 205-266.

Slavin, J. A., E. J. Smith, D. G. Sibeck, D. N. Baker, R. D. Zwickl, and S. Akasofu (1985), An ISEE 3 study of average and substorm conditions in the distant magnetotail, *J Geophys Res: Space Physics*, *90*(A11), 10875-10895.

Snekvik, K., E. Tanskanen, N. Østgaard, L. Juusola, K. Laundal, E. I. Gordeev, and A. L. Borg (2012), Changes in the magnetotail configuration before near-Earth reconnection, *J Geophys Res: Space Physics*, *117*(A2), n/a-n/a.

Sun, W., S. Fu, Q. Shi, Q. Zong, Z. Yao, T. Xiao, and G. Parks (2014), THEMIS observation of a magnetotail current sheet flapping wave, *Chinese Sci. Bull.*, 59(2), 154-161.

Walsh, A. P., C. J. Owen, A. N. Fazakerley, C. Forsyth, and I. Dandouras (2011), Average magnetotail electron and proton pitch angle distributions from Cluster PEACE and CIS observations, *Geophys Res Lett,* 38(L06103).

Wang, C., L. R. Lyons, T. Nagai, and J. C. Samson (2004), Midnight radial profiles of the quiet and growth-phase plasma sheet: The Geotail observations, *J Geophys Res: Space Physics*, *109*(A12), n/a-n/a.

Wang, C., M. Gkioulidou, L. R. Lyons, and V. Angelopoulos (2012), Spatial distributions of the ion to electron temperature ratio in the magnetosheath and plasma sheet, *J Geophys Res: Space Physics*, 117(A8), n/a-n/a.

Wang, C., C. Yue, S. Zaharia, X. Xing, L. Lyons, V. Angelopoulos, T. Nagai, and T. Lui (2013), Empirical modeling of plasma sheet pressure and three-dimensional force-balanced magnetospheric magnetic field structure: 1. Observation, *J Geophys Res: Space Physics*, *118*(10), 6154-6165.

Xing, X., L. R. Lyons, V. Angelopoulos, D. Larson, J. McFadden, C. Carlson, A. Runov, and U. Auster (2009), Azimuthal plasma pressure gradient in quiet time plasma sheet, *Geophys. Res. Lett.*, *36*(L14105).

Xing, X., L. R. Lyons, Y. Nishimura, V. Angelopoulos, E. Donovan, E. Spanswick, J. Liang, D. Larson, C. Carlson, and U. Auster (2011), Near-Earth plasma sheet azimuthal pressure gradient and associated auroral development soon before substorm onset, *J Geophys Res: Space Physics*, *116*(A7), n/a-n/a.

Yao, Z. H., et al. (2012), Mechanism of substorm current wedge formation: THEMIS observations, *Geophys. Res. Lett.*, 39, L13102, doi:10.1029/2012GL052055.

Yue, C., C. Wang, Y. Nishimura, K. R. Murphy, X. Xing, L. Lyons, M. Henderson, V. Angelopoulos, A. T. Y. Lui, and T. Nagai (2015), Empirical modeling of 3-D force-balanced plasma and magnetic field structures during substorm growth phase, *J Geophys Res: Space Physics*, *120*(8), 6496-6513.

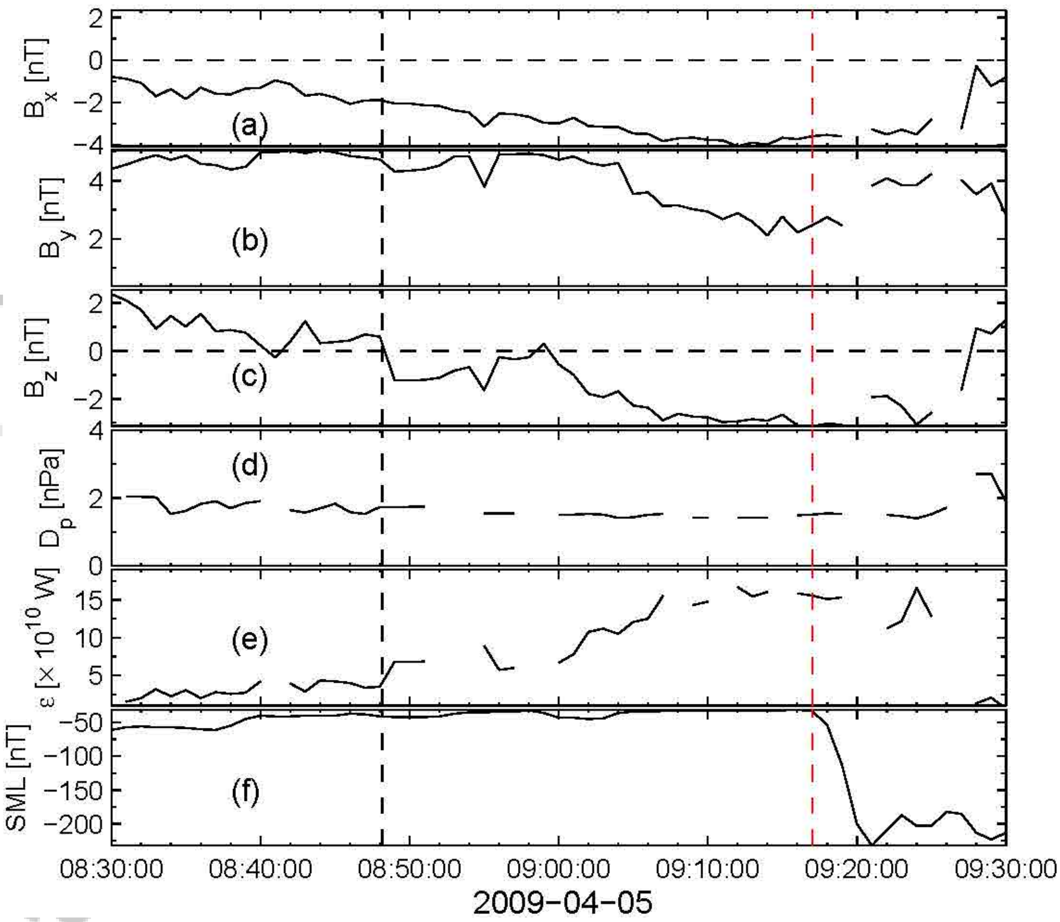

Figure 1. Overview of the solar wind and geomagnetic perturbations. (a) Interplanetary magnetic field (IMF) *X* component (B_x), (b) IMF B_y, (c) IMF B_z, (d) solar wind dynamic pressure (D_p), (e) energy input from the solar wind to the magnetosphere (ϵ) [*Perreault and Akasofu*, 1978], and (f) the SuperMAG SML indices (similar to AL) [*Gjerloev*, 2012]. The first vertical dashed line (black) indicates the southward turning of IMF, i.e., beginning of substorm growth phase. The second (red) vertical dashed line represents the onset of expansion phase based on the criteria from *Newell and Gjerloev* [2011].

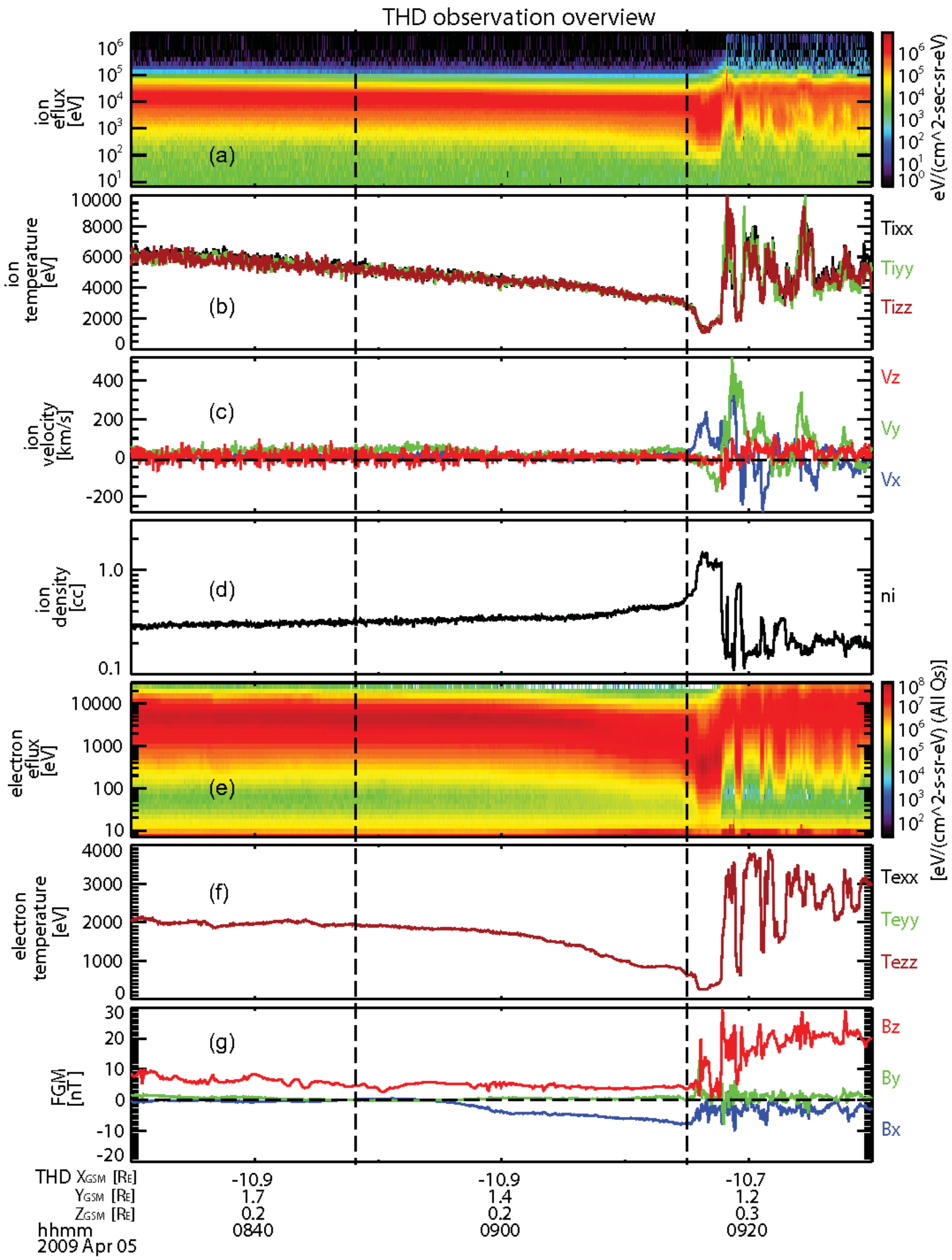

Figure 2. Overview of THD particle and magnetic field observations. (a) Energy spectrum for ion differential energy flux, (b) diagonal components of ion temperature tensor, T_{ixx} (black), T_{iyy} (green) and T_{izz} (red), (c) ion velocity components, V_x (blue), V_y (green) and V_z (red), (d) ion density (n_i), (e) Energy spectrum for electron differential energy flux, (f) diagonal components of electron temperature tensor, T_{exx}

(black), T_{eyy} (green) and T_{ezz} (red), and (g) magnetic field components, B_x (blue), B_y (green) and B_z (red). Ions spectrum and moments are from the combination of ESA and SST measurements, while electrons are from ESA measurements. The first vertical dashed line corresponds to the beginning of substorm growth phase. The second vertical dashed line represents the beginning of substorm dipolarization. See text for detail descriptions.

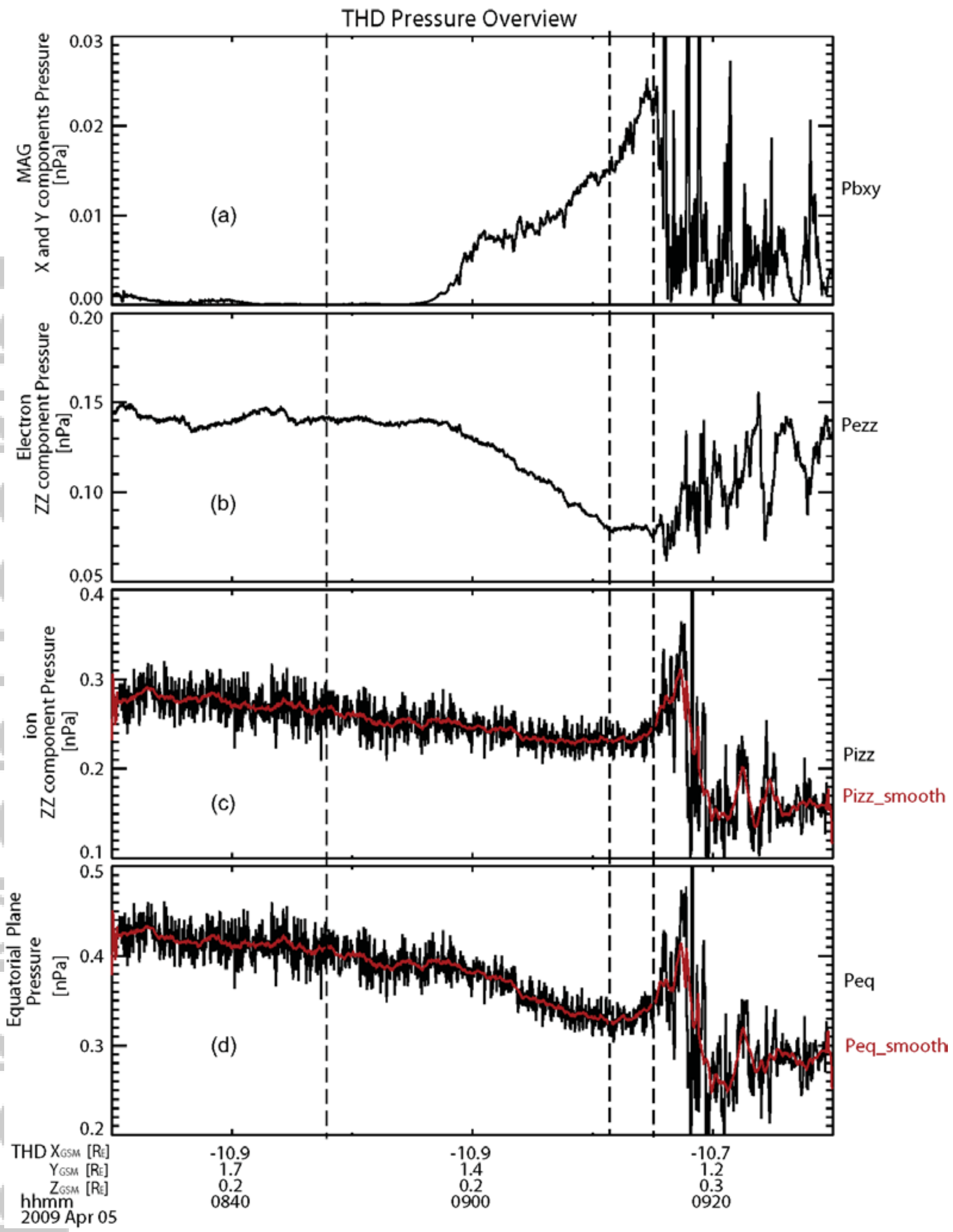

Figure 3. Overview of pressure variations from THD observations. (a) Magnetic pressure of B_x and B_y components (P_{bxy}), (b) electron *zz* component pressure (P_{ezz}), (c) ion *zz* component pressure (P_{izz}), and (d) the equatorial plasma pressure (P_{eq}). Red lines in (c) and (d) are one minute moving means of the data. The first and last vertical dashed lines correspond to the beginning and end of substorm growth phase, respectively. The second vertical dashed line indicates the time of minimum P_{eq}.

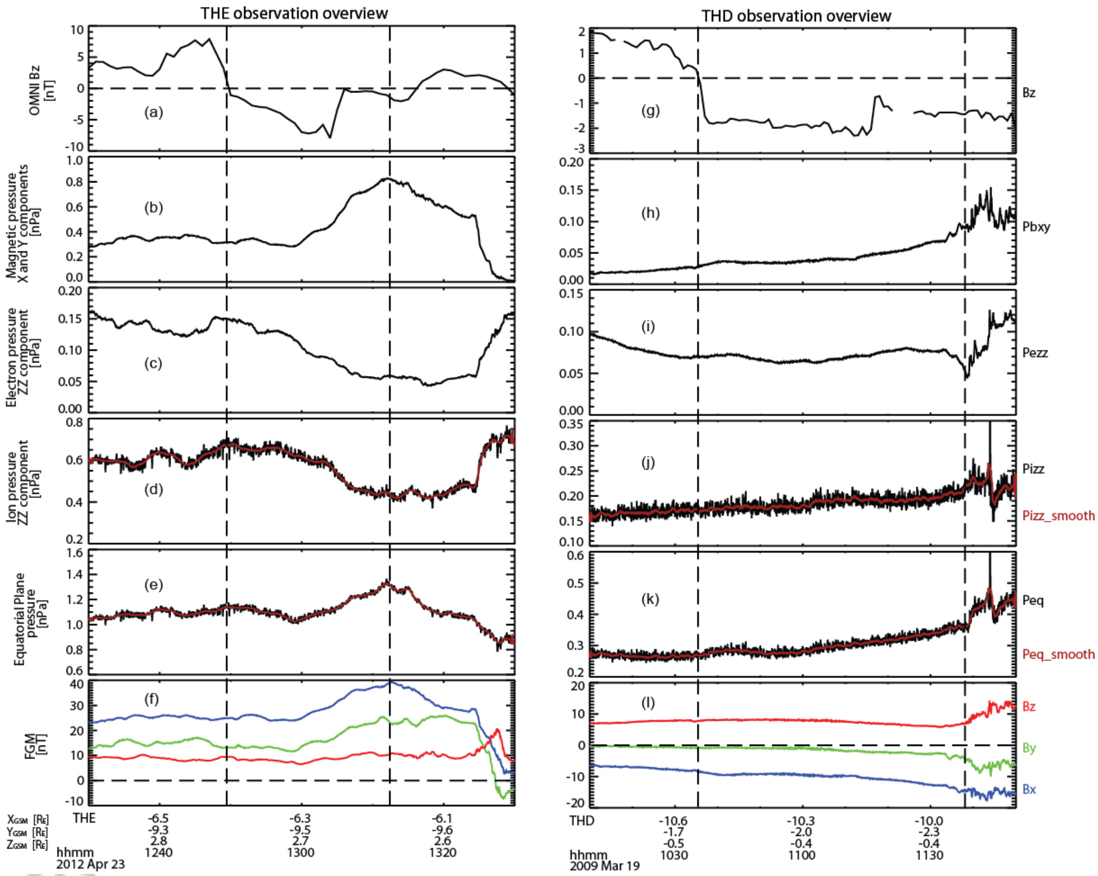

Figure 4. Left column: overview of a substorm growth phase event located in the near dawn flank region from THE. Right column: overview of an event with equatorial plasma pressure increase from THD. (a, g) IMF B_z, (b, h) P_{bxy}, (c, i) P_{ezz}, (d, j) P_{izz}, (e, k) P_{eq}, and (f, l) B_x (blue), B_y (green) and B_z (red). Red lines in (d), (e), (j) and (k) are one minute moving means of the data. The first and last vertical dashed lines in each event correspond to the beginning and end of substorm growth phases.

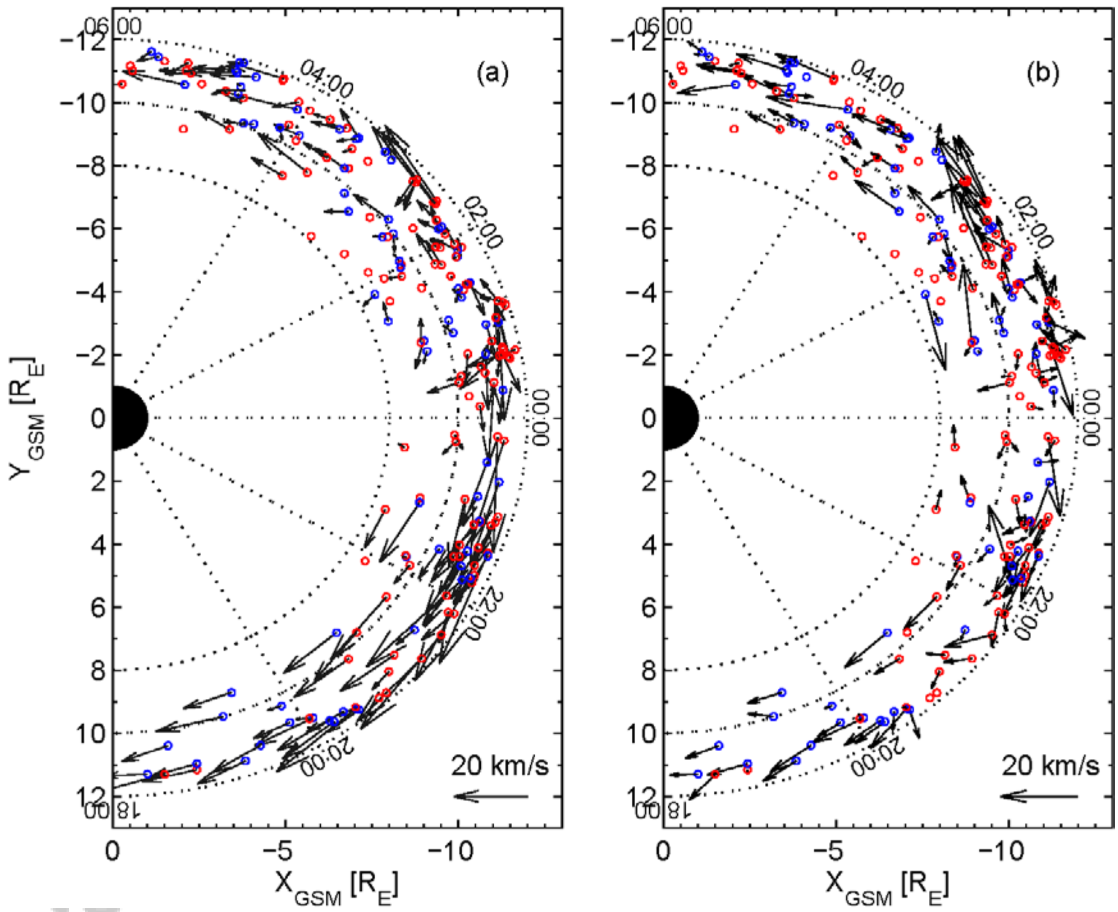

Figure 5. Statistical features of equatorial plasma pressure (P_{eq}) and plasma flows for the 193 probes observations in the X_{GSM}-Y_{GSM} plane. (a) Blue circles represent the probe locations for cases observed the phenomenon of P_{eq} decrease during the substorm growth phase. Red circles represent the locations for other cases. Black arrows indicate the averaged plasma flows V_x and V_y components ($V_x\vec{e}_x + V_y\vec{e}_y$) during the substorm growth phases. (b) is in the same format as (a), but with black arrows indicating the plasma flow differences ($\Delta\vec{V}_{xy}$) between flows in Figure 5a and the averaged plasma flows in half an hour prior to the start of each substorm growth phase case.

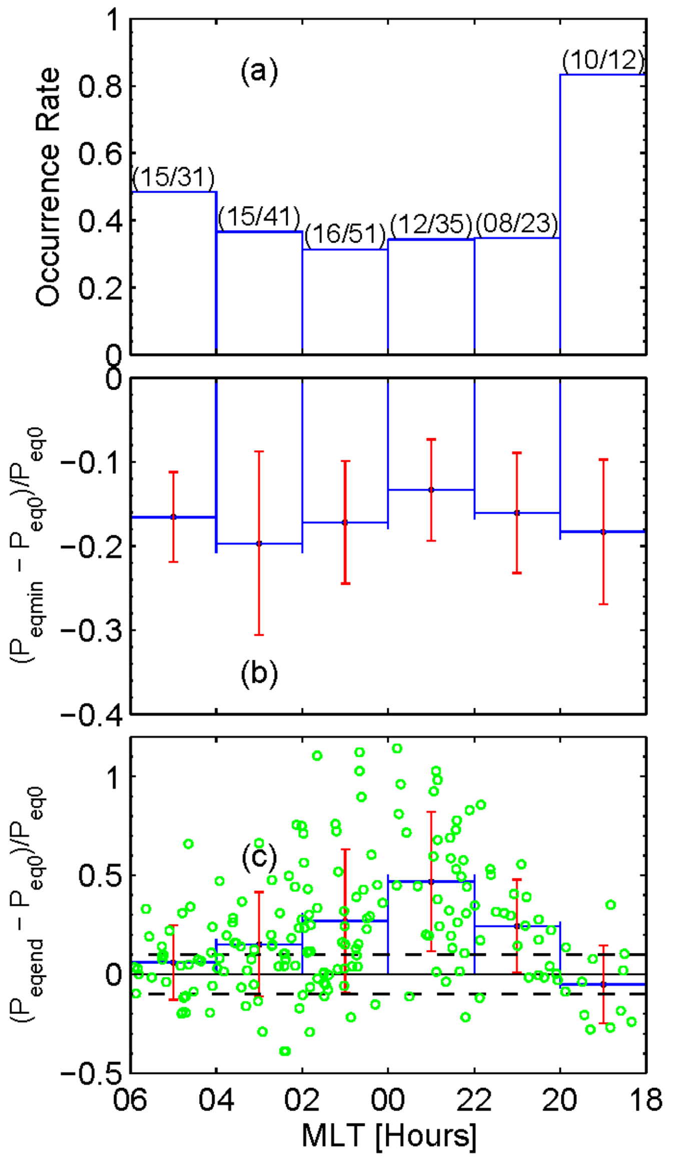

Figure 6. Statistical features on the equatorial plasma pressure (P_{eq}) variations. (a) Occurrence rates for P_{eq} decrease cases in different Magnetic Local Time (MLT) bins. (b) Distribution for the average ratios of P_{eq} decrease ((P_{eqmin} - P_{eq0}) / P_{eq0}) in each MLT bins. This figure includes the P_{eq} decrease cases. P_{eqmin} represents the minimum P_{eq} during the growth phase, and P_{eq0} the P_{eq} prior to growth phase. (c) Distribution for the average ratios of P_{eq} increase at the end of substorm growth phase ((P_{eqend} - P_{eq0}) / P_{eq0}) in each MLT bins. P_{eqend} represents the P_{eq} at the end of growth phase. Green circles are the scatter of ratios of the 193 cases. The two horizontal dashed lines represent the values of 0.1 and -0.1, respectively.

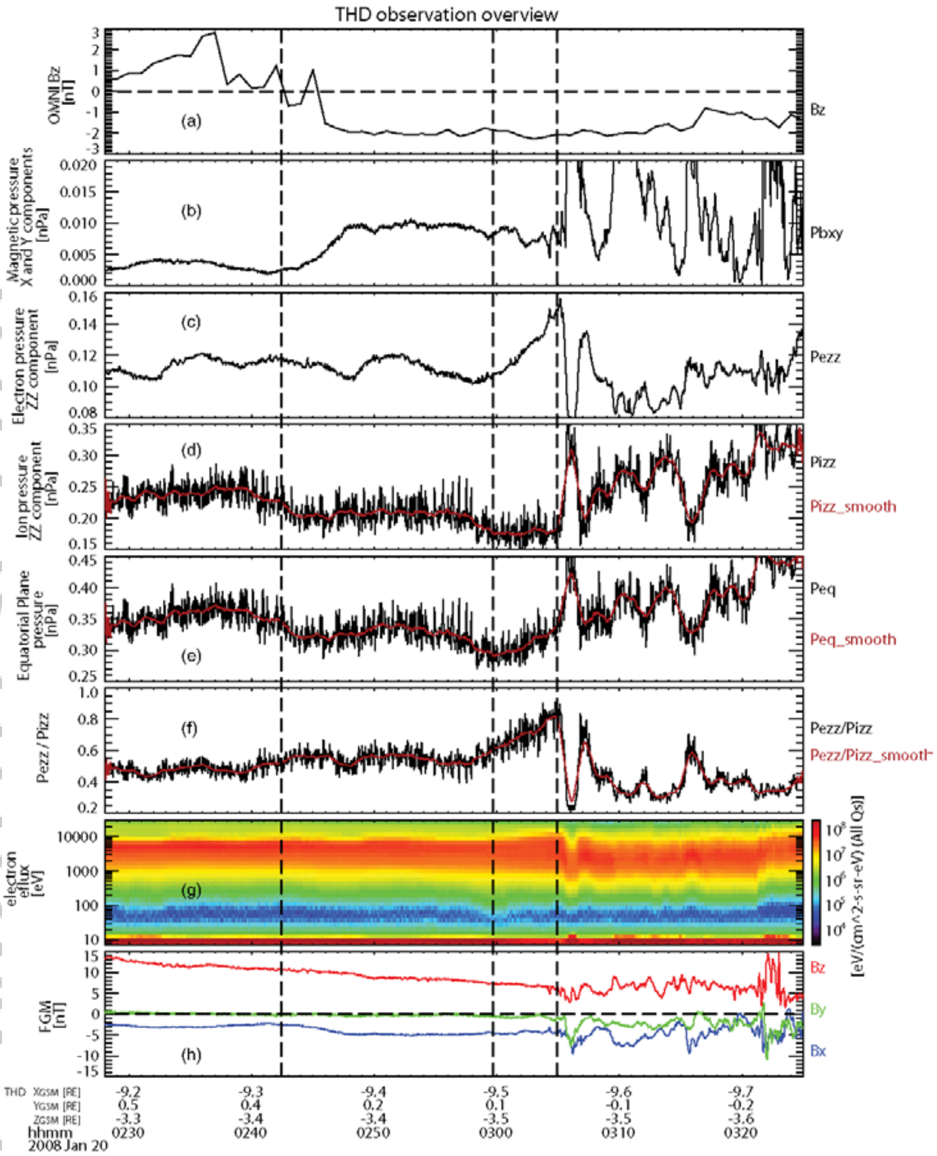

Figure 7. Overview of a substorm growth phase event from THD on 20 January 2008. (a) IMF B_z, (b) P_{bxy}, (c) P_{ezz}, (d) P_{izz}, (e) P_{eq}, (f) ratios between P_{ezz} and P_{izz}, (g) energy spectrum for electron differential energy flux from ESA, and (h) B_x (blue), B_y (green), and B_z (red). Red lines in (d), (e) and (f) are 1 minute moving mean of the data. The first and last vertical dashed lines represent the beginning and end of this substorm growth phase, respectively, and the middle line indicates the time when P_{eq} reaches the minima.

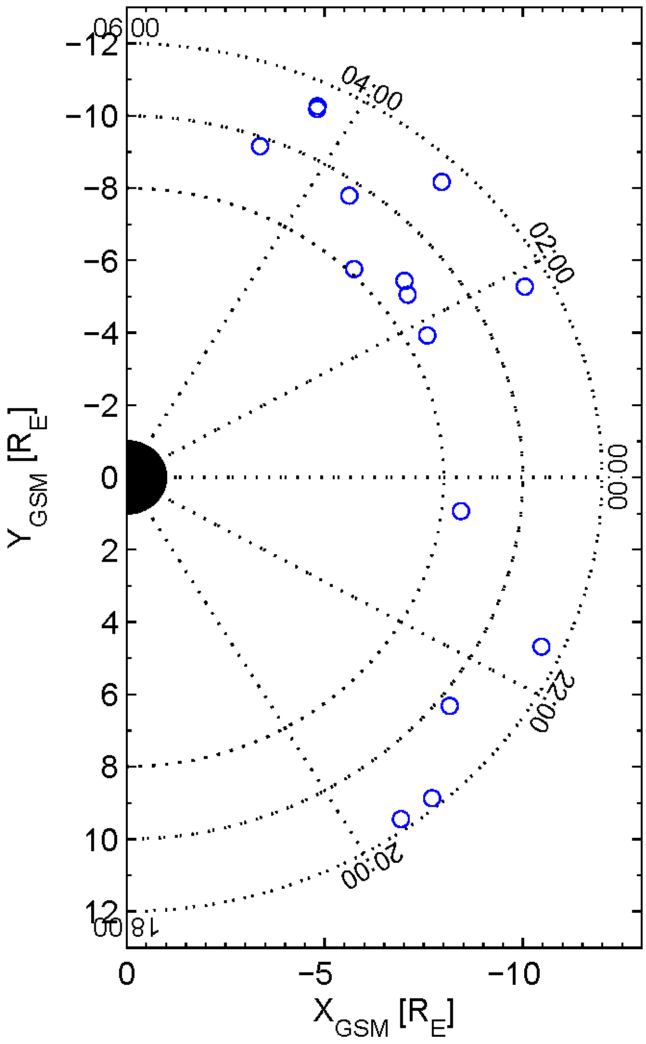

Figure 8. The distribution of the 15 cases of large electron pressure contributions (with the ratios of ΔP_{ezz} to ΔP_{eq} larger than 50%) in the X_{GSM}-Y_{GSM} plane. Each circle indicates a single event.

Table 1. The list of substorm growth phase events for electron pressure variations [a]

#	date (UT)	probe	P_{bxy} changes (ΔP_{bxy}, nPa)	P_{ezz} changes (ΔP_{ezz}, nPa)	P_{eq} changes (ΔP_{eq}, nPa)	P_{izz} changes (ΔP_{izz}, nPa)	P_{ezz}/P_{izz} changes	Group[b]
1	13 December 2007, 03:39 to 04:30	THD	~ 0.023	~ 0.12	~ 0.13	~ -0.059	~ 63.4%	Third
2	20 December 2007, 03:15 to 03:57	THD	~ 0.01	~ -0.12	~ -0.11	~ -0.20	~ 61.7%	First
3	23 December 2007, 09:30 to 10:09	THE	~ -0.0045	~ 0.023	~ 0.029	~ -0.079	~ 35.9%	First
4	20 January 2008, 02:42 to 03:05	THD	~ 0.005	~ 0.045	~ 0.23	~ 0.14	~ 55%	NaN
5	03 March 2008, 03:48 to 04:30	THA	~ 0.02	~ 0.19	~ 0.052	~ -0.14	~ 50%	Third
6	10 April 2008, 04:50 to 05:22	THD	~ -0.004	~ 0.063	~ -0.004	~ 0.056	~ -11.3%	Second
7	10 April 2008, 04:50 to 05:22	THE	~ -0.002	~ 0.064	~ 0.11	~ 0.12	~ 21%	Third
8	04 March 2009, 02:05 to 02:30	THE	~ 0.012	~ 0.098	~ 0.21	~ 0.28	~ 20%	NaN
9	14 April 2009, 06:30 to 08:05	THE	~ 0.007	~ 0.037	~ 0.045	~ -0.065	~ 33%	Third
10	28 March 2010, 15:03 to 16:16	THD	~ 0.031	~ 0.18	~ 0.19	~ 0.036	~ 96.8%	Third
11	13 March 2011, 16:08 to 17:08	THD	~ -0.005	~ 0.092	~ 0.082	~ 0.21	~ -20.2%	Third
12	13 March 2011, 16:08 to 17:08	THE	~ -0.004	~ 0.084	~ 0.14	~ 0.20	~ -23.4%	Third
13	17 March 2011, 17:59 to 19:29	THA	~ -0.004	~ 0.10	~ 0.12	~ 0.30	~ 87.0%	Third
14	3 May 2011, 16:50 to 17:18	THE	~ 0.006	~ 0.04	~ 0.028	~ -0.036	~ 66.4%	Second
15	15 August 2012, 19:19 to 21:05	THD	~ -0.007	~ 0.11	~ 0.17	~ 0.20	~ 51.7%	Third
16	7 October 2012, 17:03 to 18:37	THE	~ 0.009	~ -0.052	~ -0.13	~ -0.18	~ -16.7%	NaN
17	4 September 2014, 22:07 to 23:33	THE	~ 0.009	~ 0.15	~ 0.0038	~ 0.044	~ 77.4%	Third
18	25 September 2014, 18:22 to 18:53	THD	~ -0.01	~ 0.06	~ 0.15	~ 0.16	~ 37.1%	NaN
19	25 September 2014, 18:22 to 18:53	THE	~ 0.014	~ 0.07	~ 0.037	~ 0.039	~ 21.6%	Second

a. The events with $|\Delta P_{ezz}|/|\Delta P_{bxy}| \geq 5$, and $P_{ezz}/P_{bxy} \geq 5$

b. Group is defined in section 2.3.

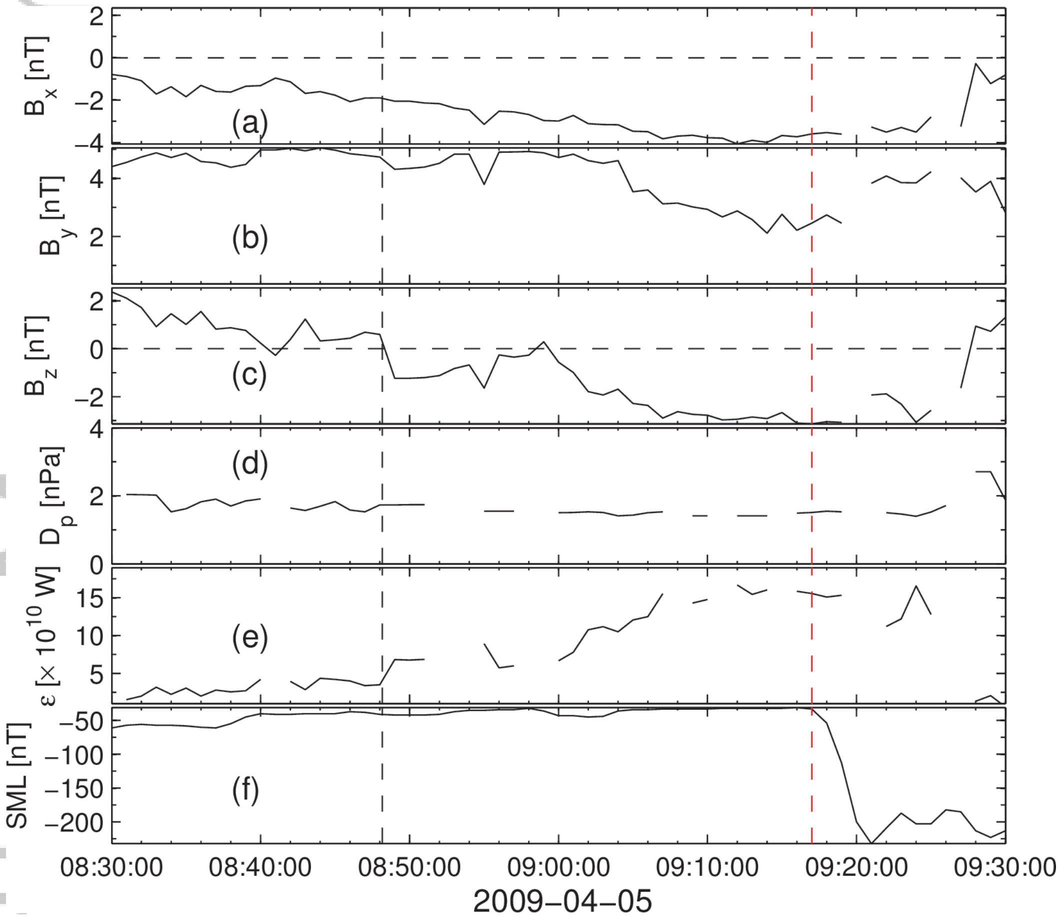

2017ja024603-f01-z-.eps

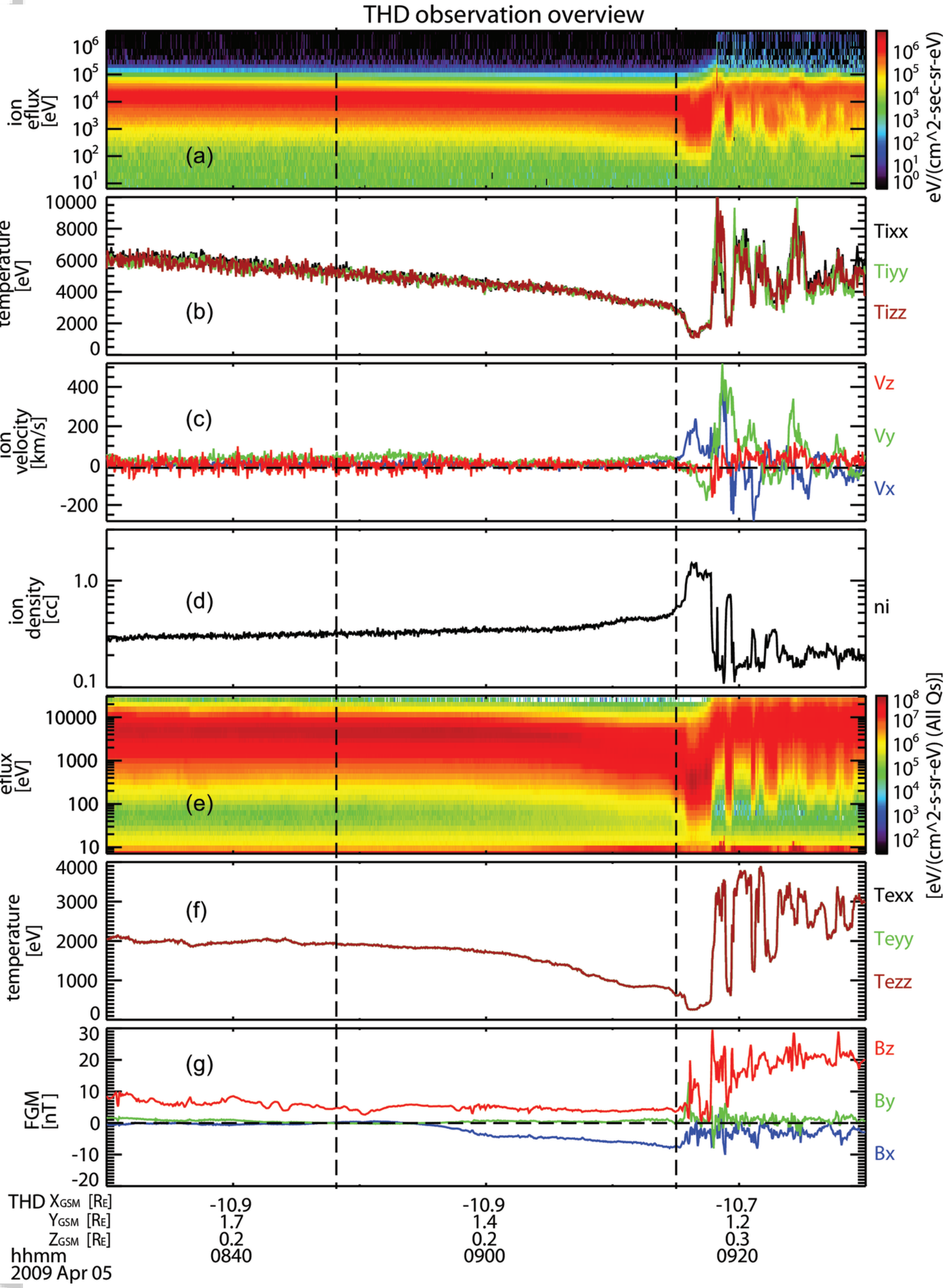

2017ja024603-f02-z-.eps

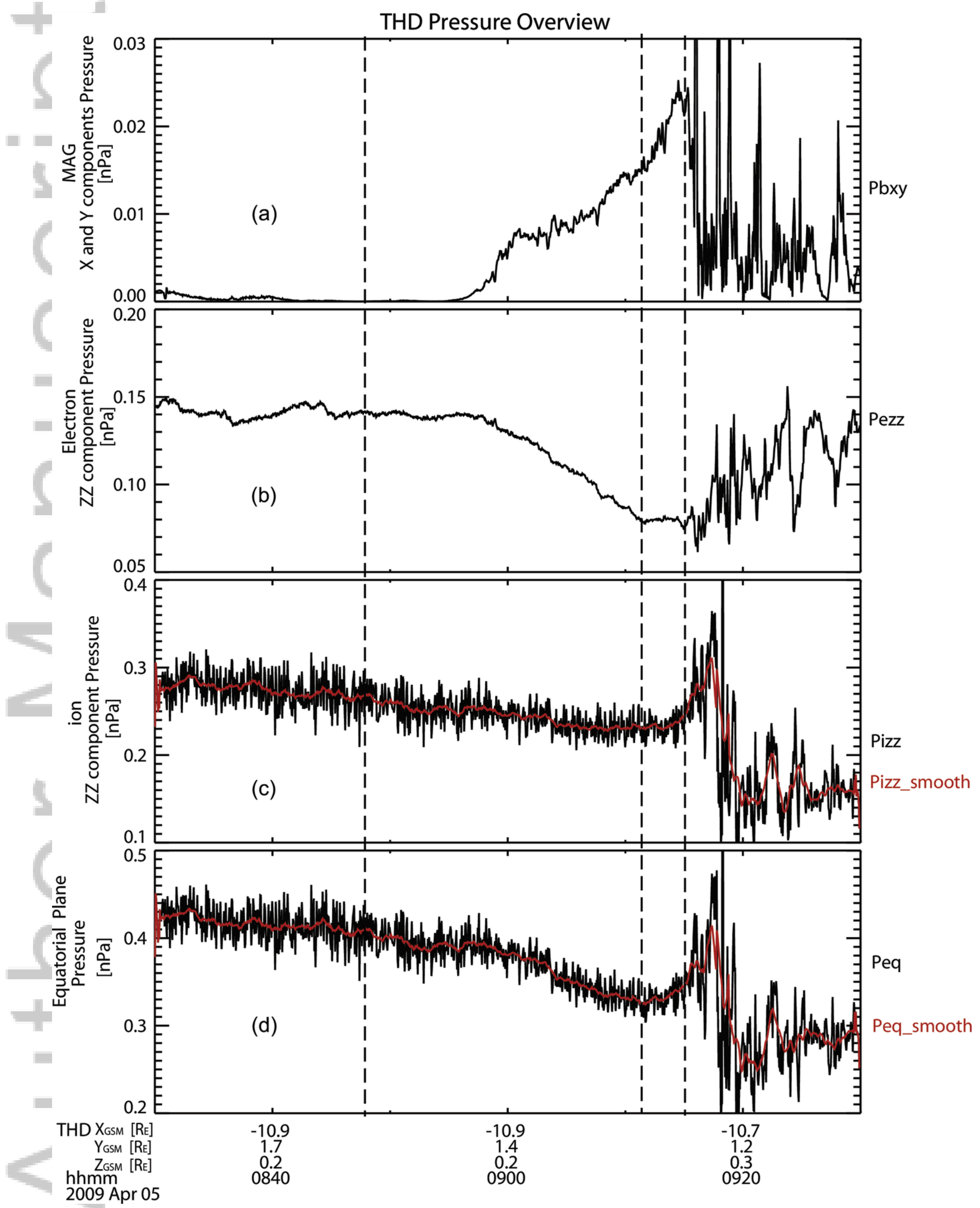

2017ja024603-f03-z-.eps

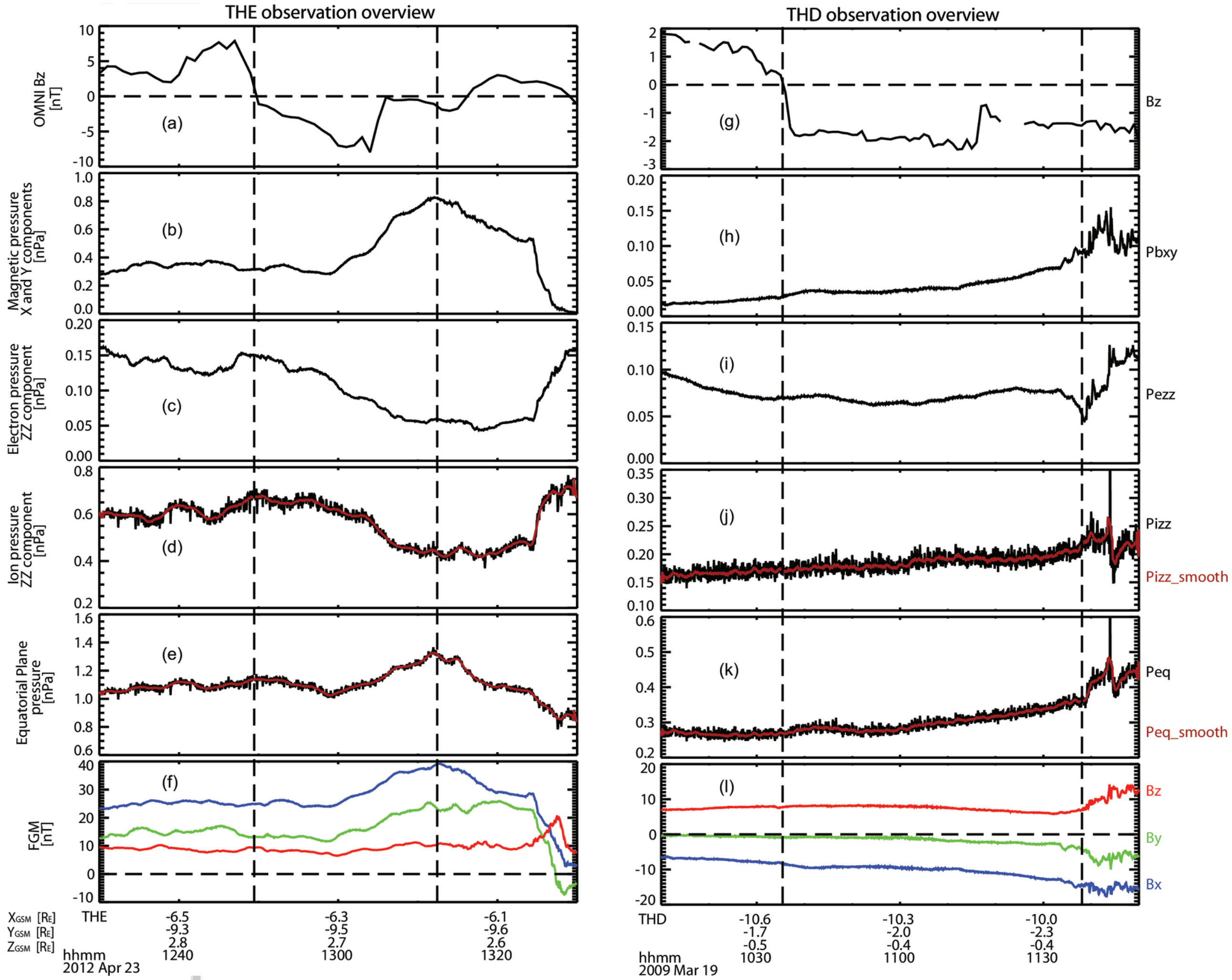

2017ja024603-f04-z-.eps

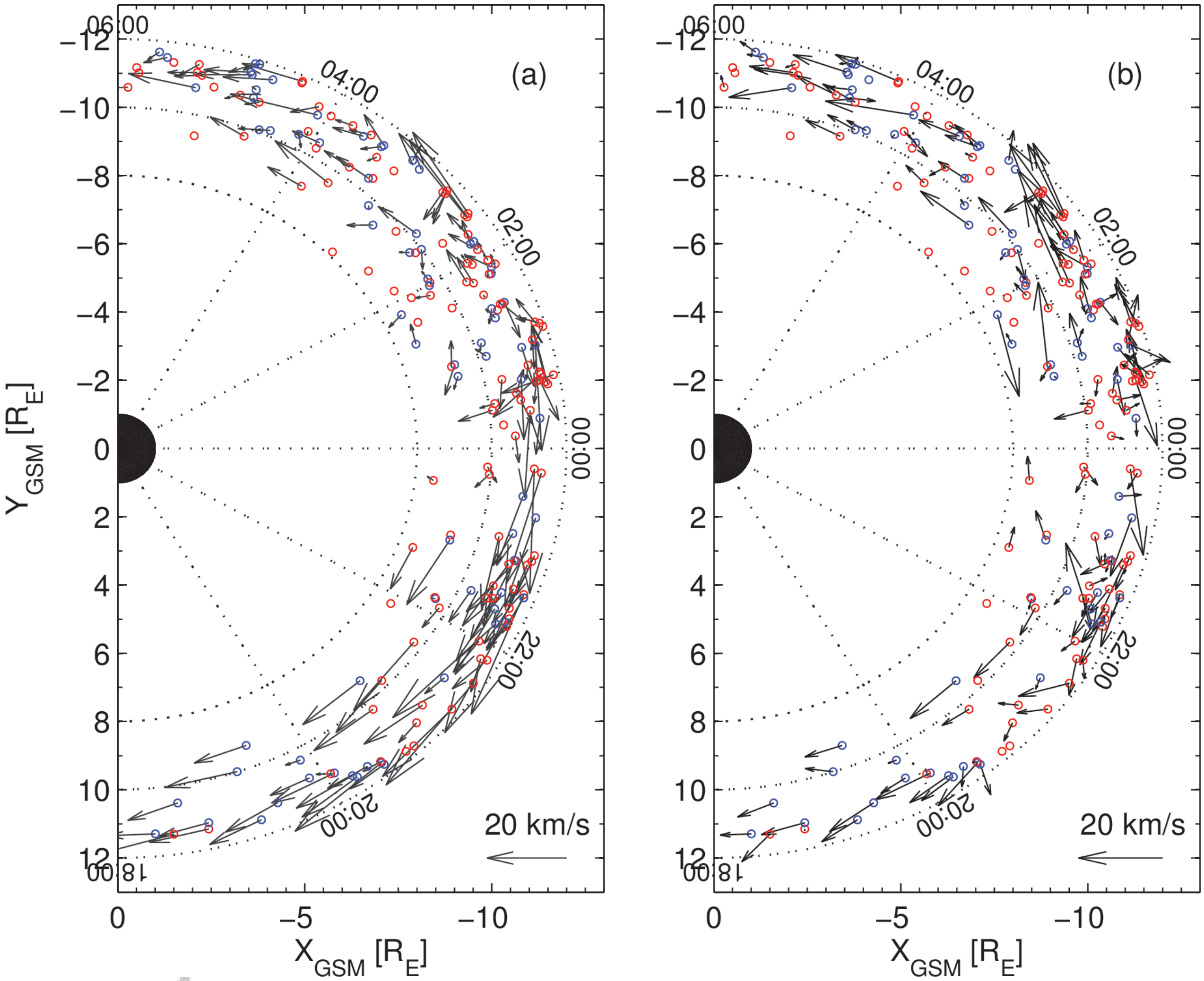

2017ja024603-f05-z-.eps

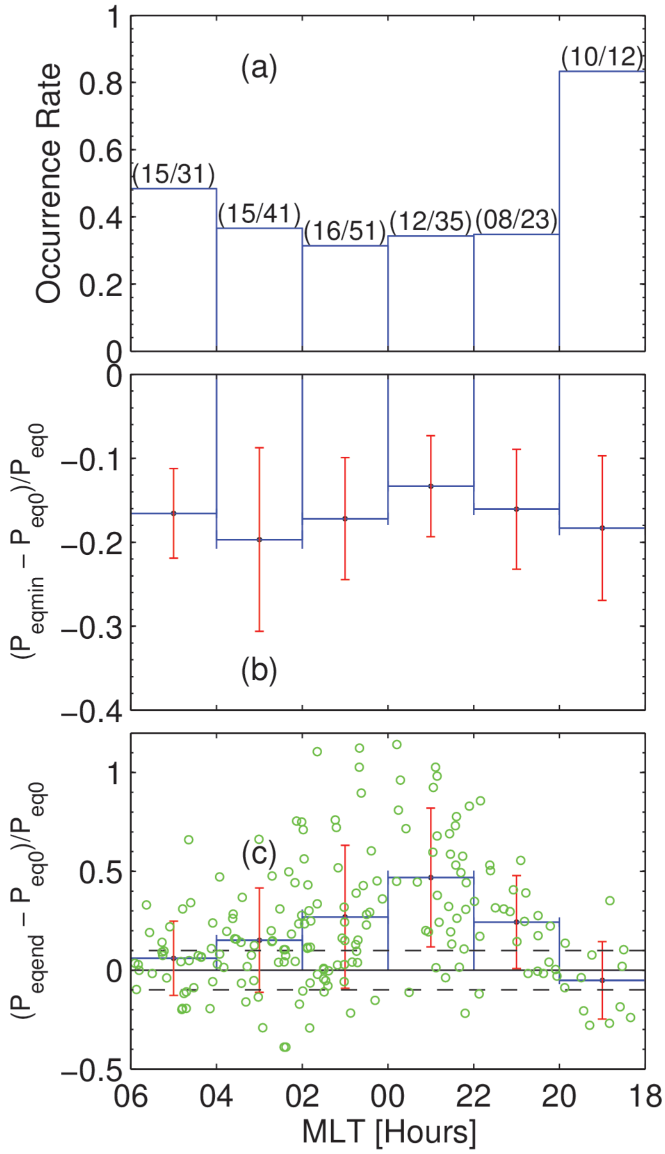

2017ja024603-f06-z-.eps

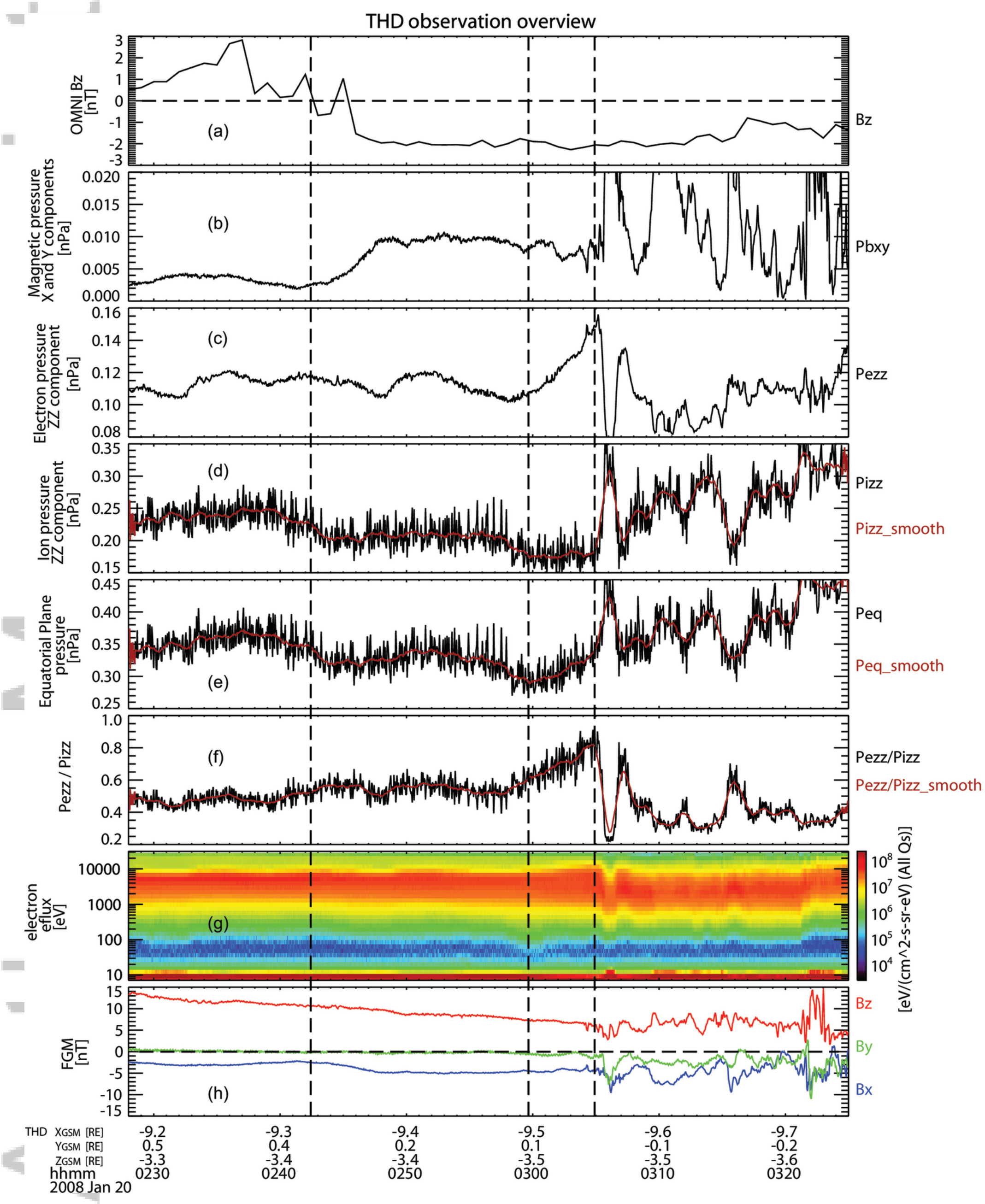

2017ja024603-f07-z-.eps

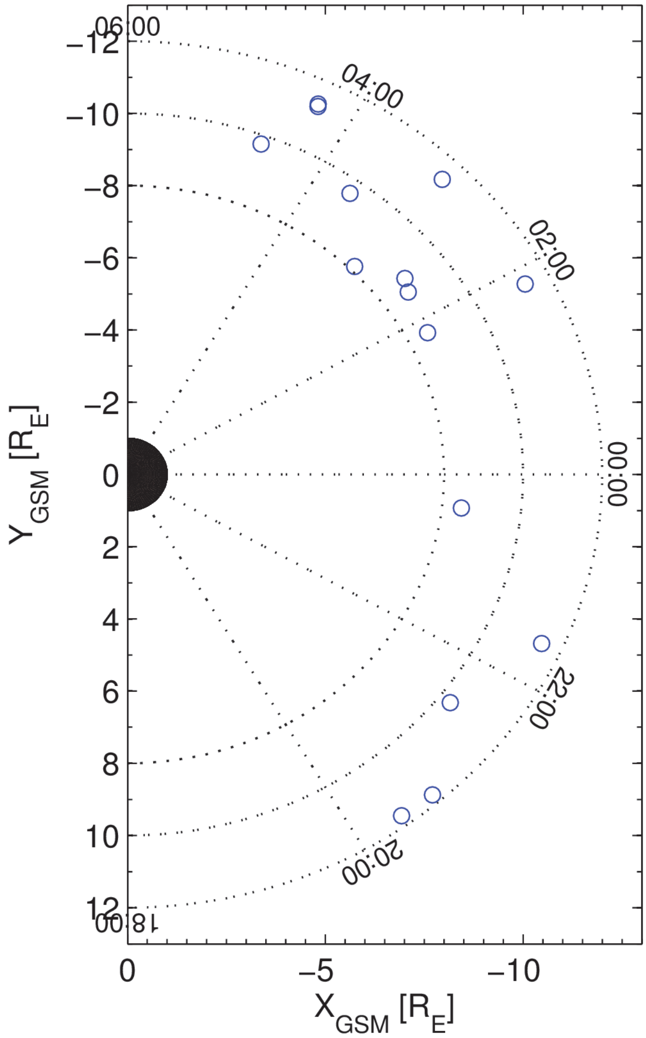

2017ja024603-f08-z-.eps